This manuscript has been published online in: Received 6 March 2025, Revised 29 May 2025, Accepted 19 June 2025, Available online 25 June 2025, Version of Record 12 July 2025.

 $\underline{https://doi.org/10.1016/j.dental.2025.06.017}$ 

ELSEVIER

Contents lists available at ScienceDirect

### **Dental Materials**

journal homepage: www.elsevier.com/locate/dental





## Polymeric nanocarriers doped with a parathyroid hormone-related protein enhances dentin apposition and nanohardness at the resin-dentin interface

Manuel Toledano<sup>a</sup>, Fátima S. Aguilera<sup>a,\*</sup>, Marta Reinoso<sup>b</sup>, María T. Osorio<sup>a</sup>, Raquel Toledano<sup>a</sup>, Christopher D. Lynch<sup>c</sup>, Estrella Osorio<sup>a</sup>

- <sup>a</sup> University of Granada, Faculty of Dentistry, Colegio Máximo de Cartuja, Granada 18071, Spain
- <sup>b</sup> University of Granada, Faculty of Pharmacy, Campus de Cartuja, Granada 18071, Spain
- <sup>c</sup> University Dental School & Hospital/Cork University Dental School & Hospital, Cork, Ireland

#### ARTICLE INFO

Keywords:
Hardness
SEM
Dentin
Collagenase
Mechanical
Confocal
Nanoparticles
Microtensile bond strength
PTH
Remineralization

#### ABSTRACT

Objectives: Restoring the original composition and properties of damaged tissues is aimed by regenerative medicine. The objective of the study was to assess remineralization and bonding capabilities of etched dentin treated with polymeric nanoparticles (NPs) functionalized with parathyroid hormone related proteins (PTHrP). *Methods*: Dentin etched surfaces were treated with NPs and PTHrP-NPs. The created bonded interfaces were stored for 24 h and further submitted to thermal, chemical and mechanical challenging. Interfaces were assessed through microtensile bond strength, nanohardness, Raman analysis, a fluorescent technique with a confocal laser scanning microscopy, and scanning electron microscopy.

Results: Surfaces of dentin treated with PTHrP-NPs and load cycling or immersed in collagenase showed higher bond strength than the other groups. PTHrP promoted the highest nanohardness and phosphate peak intensity at the interface when load cycling was applied. Both porosity and nanoleakage were declined after PTHrP-NPs infiltration. Dentinal tubule walls and hybrid layer showed the strongest signals of xylenol orange stain.

Conclusions: The highest dentin bonding efficacy was obtained in samples treated with PTHrP-NPs, as they inducted the greatest remineralization measured by nanoindentation and Raman analysis, high values of bond strength and advanced mineral deposition at the resin-dentin interface and tubules. PTHrP-NPs enabled sealing with scarce nanoleakage and porosity at the interface.

Significance: Etched dentin infiltration with hydrophilic polymeric NPs functionalized with parathyroid hormone related proteins, poses an advance in regenerative dentistry, by developing therapeutic bioactivity.

#### 1. Introduction

In biomineralized tissues, such as dentin, which is a major component of teeth, the apatite crystals that perform as filler particle stiffen the collagen matrix [1]. Adhesive dentistry attempts to entirely infiltrate the resin throughout the total thickness of the etched dentin that results after apatite removal during dentin demineralization, to form the hybrid layer (HL) [2,3]. The ideal HL may be classified as a 3-dimensional polymer/collagen network that provides a continuous and stable link between the bulk adhesive and dentin substrate. However, a high quality and durable HL can be only achieved if the demineralized dentin collagen matrix is fully resin-infiltrated [4,5]. There is a gradual resin diffusion into the demineralized dentin from the top to the bottom of the hybrid layer (BHL). The decreased gradient concentration of the

adhesive resin at the BHL, the Achilles heel of the interface, leaves collagen fibrils unprotected and vulnerable [6], after lacking the protection of the cured resin [7,8]. The absence of this resin cover also may conduct to degradation of demineralized collagen fibrils [7]. This degradation is mediated by endogenous matrix metalloproteinases, in junction with their extracellular inhibitors. Some *in vitro* methods for testing consequences of aging involve challenging the resin-dentin interface with load cycling or testing the resistance of the resin-dentin interfaces when subjected to hydrolytic degradation under thermal stresses. Load cycling and thermocycling of bonded specimens have been widely employed for *in vitro* assessment of resin-based dental materials [9], simulating the oral environment [10] and have been incorporated in the present methodology. The development of innovative bioactive materials with a therapeutic effect on the mineral-depleted

<sup>\*</sup> Correspondence to: University of Granada, Faculty of Dentistry, Dental Materials Section, Colegio Máximo de Cartuja, Granada 18071, Spain. E-mail address: fatimas@ugr.es (F.S. Aguilera).

sites within the bonded-dentin interface remains one of the main targets of the dental biomaterial research [11]. Dentin may undertake a remineralization process at this insufficiently infiltrated resin-dentin interface, due to its strong capacity for regeneration following damage [7,8, 12].

As phosphate- and calcium- sequestering materials, polymeric nanoparticles (NPs) have been postulated to generate mineral deposits at the demineralized dentin. These NPs are non-resorbable and biocompatible biomaterials, made of methacrylic acid, ethylene glycol dimethacrylate and 2-hydroxyethyl methacrylate, covalently linked [13]. Anionic carboxylate groups (i.e., COO-) are present in the chemical formulation of these NPs, permitting functionalization with drugs containing amino groups or metal cations [14], or biomimetic peptides that facilitate dentin remineralization [15]. Polymeric NPs, at the resin-dentin interface, are capable to attach to the collagen favoring the precipitation of precursors of amorphous calcium-phosphate, helping to promote tissue mineralization [16]. Engineered NPs represent a key-point of much investigation in the remineralization field, as they may serve as carriers for other biological factors [17].

A diversity of signaling molecules have been studied for their capability to induce dentin remineralization and regeneration. Parathyroid hormone or parathormone (PTH) is a peptide which has been indicated, in the present research, as a potential candidate to facilitate dentin remineralization [18]. The parathyroid glands secret the PTH, which is a polypeptide containing 84 amino acids. PTH, essentially, regulates the calcium and phosphate homeostasis [19]. It has been demonstrated that PTH shows an anabolic effect in bone, maxillary tissues and teeth [20]. Furthermore, PTH generates calcified dentin [21] and may help to reparative dentin formation. More recently, PTH has been recommended for inducing dentin formation [22].

The classic actions of PTH is located in the N-terminal (1–34 region) of the peptide. PTH acts throughout the type 1 PTH receptor (PTHR1), a g-protein coupled receptor, that activates several interrelated pathways that lead to increased multiple survival signaling [19]. The principal procedure that facilitates the PTH anabolic action is the cyclic adenosine monophosphate (c-AMP)-signaling of the protein kinase response to the activation of PTHR1 [23,24]. Anabolic properties are also linked to the effect that PTH shows on local factors like TGF\$\beta\$ or Wnts through endocytosis and/or recruitment of their receptors to PTHR1 [25]. Reparative dentin formation is positively regulated by Wnt signaling cascades [26], playing an important role in dentin patterning [27]. PTH has been widely indicated to treat osteoporosis, and to facilitate osseointegration of implants [18]. PTH can promote mineralization by forming mineral nodules, increasing the secretion of osteocalcin and ALP activity. Hence, peptides and proteins are activated, confirming the odontogenic potential of PTH and showing the clinical benefit in dentin regeneration [22]. PTH can, therefore, generate calcified dentin [21] contributing to reparative dentin formation in restorative dentistry [26].

The manner of administration determines the effects of PTH [19]. Alterations in PTH serum level conduct to formation of abnormal dentin [28] and resorption [29]. It has been also shown that PTH can stimulate apposition of dentin in rats that were thyroparathyroidectomized, in a dose-dependent manner [30]. Local addition of PTH has enhanced bone regeneration [31]. In an attempt to optimize clinical efficacy of PTH application, the peptide has been applied, first, following an intermittent systemic administration, but this modality requires a daily/weekly self-injection, very often is exposed a not-target area and achieves a mild side-effect [32]. Local single doses of PTH have also been proposed, but without clinical effects at any evaluated time-point [18]. Thereby, in situ delivery for a constant presence of PTH to a local environment has been raised in the present work. Recent investigations have tried to include PTH into hydrogels [25], ceramics [33], and even on titanium by forming hyaluronic acid multilayers to promote bone formation [34]. Synthetic matrices containing PTH for bone formation were, first, used but differences between experimental and control groups were not found [35]. A plasmin sensitive link of a fibrin gel associated to PTH

was, then, utilized, but the methodology to proceed resulted excessively sophisticated [36]. PTH has also been associated to xenografts [37] or combined with octacalcium phosphate and collagen composite [38]. A self-assembling peptide nanofiber hydrogel locally delivered (SPG-178) and systemic PTH have been tested to treat periodontal defects, producing differentiation, angiogenesis and increased cell proliferation [24]. In any case, emphasis should be applied in optimizing the local administration of PTH in order to promote a hard tissue healing reaction eliminating or diminishing systemic PTH response. To reduce the burst release of PTH more than relying on simple diffusive processes [39], nanocarriers, as hydrophilic polymeric NPs, have been proposed to fabricate PTH-doped NPs (PTH-NPs).

Restoring the original properties, function, and compositions of lost and damaged tissues poses the definitive target of regenerative medicine [40]. Parathyroid hormone-related protein (PTHrP), the peptide that was used in the present research, is similar to PTH functionally and structurally [22]. The remineralizing potential of PTHrP has never been stated. Therefore, effective systems for PTH administration at the desired local dentin site, can help to preserve PTHrP bioactivity, and induced optimal dentin activity might be a challenge for dentin regeneration purposes. In the present manuscript, the new approach to address the scientific problem of protecting the demineralized collagen after dentin conditioning consists of using nano-carried parathyroid hormone to promote dentin mineralization after the insufficient adhesive infiltration that is produced at the resin-dentin interface when acid conditioning. The potential for in vitro dentin remineralization has, specifically, been determined by using nanohardness, as a direct method of research. The null hypotheses to be proved are that PTH-NPs infiltration into conditioned dentin did not affect the remineralization of dentin, referred to (1) efficacy of bond and morphological variations, (2) the nanomechanical performance at the interface.

#### 2. Materials and methods

#### 2.1. Nanoparticles fabrication and characterization

The nanoparticles were obtained by the polymerization precipitation method. A thermo-dynamic approach, the Flory-Huggins model, controlled the precipitation process [41]. 2-hydroxyethyl methacrylate (HEMA) (0.137 mL), methacrylic acid (MAA) (0.045 mL) and ethylene glycol dimethacrylate (EDMA) (0.170 mL) (Sigma-Aldrich, Chemie Gmbh, Riedstr, Germany) were used. Azobis-isobutyronitrile (AIBN) (8.75 mg) was added to the compound that was sonicated, and then cooled at 8 °C. N2 flow was, then, applied for 3 min [13]. The whole synthesis of the nanoparticles is reported in Medina-Castillo (2020) [41]. Parathyroid hormone (PTH) (Sigma-Aldrich) was used to load half of the fabricated NPs. 100 mg of NPs were immersed in 1 mL of 10 nM PTH solution, at room temperature, for 30 min, by using constant shaking (12 rpm). Once the solvent was completely evaporated, caution was taken to make sure that all the PTH was onto the NPs. Therefore, a percentage concentration of PTH in NPs of 9.5  $\times$   $10^{-5}$  % was attained. Control (1), undoped NPs (2) and PTH-NPs (3) groups were established. Z-potential was assessed by fixing in water a 5 mg/mL suspension of PTH-NPs. A dynamic light scattering (DLS) measurement (Zetasizer Nano ZS90/Malvern Instrument Ltd, Malvern, UK) was also set in triplicate. Morphological TEM characterization of the biomaterials was also provided utilizing an amount of 10 µl (1 mg/mL) on a grid; then, activated carbon was used for coating. Uranyl acetate at 2 %, was used to negatively stain the samples for visualization [42]. For image acquisition, a Fei Titan 80-300 TEM-STEM microscope (ThermoFisher Scientific, Waltham, USA) was used at 300 kV. Fourier-transform infrared spectroscopy (FTIR) analysis of both, NPs and PTH-NPs specimens was obtained with a JASCO 6200 FTIR and ATR equipment (ATR Pro ONE, JASCO Inc., Maryland, USA). The spectral resolution was 2 cm<sup>-1</sup> during 75 scans. The frequency was between 400–4000 cm<sup>-1</sup>.

# 2.2. Specimen preparation for the bonding procedure, mechanical, chemical and thermal degradation assessment

Unerupted human third molars (forty-eight) were extracted and stored, no longer than 1 month, at 4 oC in a 0.5 % chloramine T solution. Ethical approval (1906/CEIH/2020) was followed. In order to obtain sound dentin surfaces, teeth were sectioned, horizontally, below the dentin-enamel junction. Silicon carbide abrasive paper (180-grit) was employed to polish the dentin surfaces and to generate a relevant smear layer. 37 % phosphoric acid was used to etch dentin, for 15 s. Then, surfaces were rinsed and dried. The teeth were randomly assigned, by the tool http://www.randomizer.org/form.htm, to each group, according to the storage time employed and the type of NP. The following primers were applied: (i) just an ethanol solution (30 s), or (ii) an ethanol suspension of undoped NPs, and (iii) PTH-NPs (10 mg/mL) in each of the three experimental groups. A conventional adhesive protocol was followed after ethanol evaporation (30 s) and Single Bond (SB) resin (3 M ESPE, St. Paul, MN, USA) application. The incremental technique (in five 1 mm resin coats) was practiced to construct a composite (Tetric EvoCeram, Ivoclar-Vivadent AG, Schaan, Liechtenstein) build-up

Table 1
Materials used in this study and respective manufacturer's application.

Product details	Basic formulation	Mode of application
Etchant: Phosphoric acid 37 % (Braun Medical SA, Barcelona, Spain).	37 % H <sub>3</sub> PO <sub>4</sub>	Etching application for 15 s, rinse with air/ water, Blot excess water using a cotton pellet
Adhesive system: Adper™ Scotchbond™ 1 XT (SB) (3 M ESPE, St Paul, MN, USA)	Bis-GMA; HEMA; UDMA; dimethacrylates; ethanol; water-camphorquinone; photoinitiator system; methacrylate functional copolymer (polyacrylic and polyitaconic acids); silica nanofillers (5 nm; 10 %wt)	Apply 2–3 consecutive coats of adhesive (15 s) with gentle agitation; gently air thin for 5 s to evaporate solvent. Light activation (15 s)
Composite resin: Tetric EvoCeram (Ivoclar- Vivadent AG, Schaan, Liechtenstein)	Bis-GMA, UDMA, Ethoxylated Bis-EMA. Filler loading: 82 %–83 % by weight with barium aluminum silicate glass with two particle sizes, ytterbium trifluoride, and mixed oxide	Place resin composite in increments 1.0–1.2 mm. Light-cure each coat for 20 s (to build up 6 mm high).
Solution: SBFS (Simulated Body Fluid Solution) (pH=7.45)	NaCl 8.035 g (Sigma Aldrich, St. Louis, MO, USA); NaHCO <sub>3</sub> 0.355 g (Sigma Aldrich, St. Louis, MO, USA); KCl 0.225 g (Panreac Química SA, Barcelona, Spain); K <sub>2</sub> HPO <sub>4</sub> ·3 H <sub>2</sub> O 0.231 g, MgCl <sub>2</sub> ·6 H <sub>2</sub> O 0.311 g (Sigma Aldrich, St. Louis, MO, USA); 1.0 M – HCl 39 mL (Sigma Aldrich, St. Louis, MO, USA); 1.0 M, CaCl <sub>2</sub> 0.292 g (Panreac Química SA, Barcelona, Spain); Na <sub>2</sub> SO <sub>4</sub> 0.072 g (Panreac Química SA, Barcelona, Spain); Tris 6.118 g (Sigma Aldrich, St. Louis, MO, USA) 1.0 M – HCl 0.5 mL (Panreac Química SA, Barcelona, Spain); Tris 6.118 g (Sigma Aldrich, St. Louis, MO, USA) 1.0 M – HCl 0.5 mL (Panreac Química SA, Barcelona, Spain).	

Abbreviations: H<sub>3</sub>PO<sub>4</sub>: phosphoric acid; Bis-GMA: bisphenol A diglycidyl methacrylate; HEMA: 2-hydroxyethyl methacrylate; UDMA: Urethane Dimethacrylate EDTA: ethylenediaminetetraacetic acid; bisphenol A diglycidyl methacrylate ethoxylated; SBFS: simulated body fluid solution; NaCl: sodium chloride; NaHCO<sub>3</sub>: sodium bicarbonate; KCl: potassium chloride; K<sub>2</sub>HPO<sub>4</sub>·3H<sub>2</sub>O: potassium phosphate dibasic trihydrate; MgCl<sub>2</sub>·6H<sub>2</sub>O: magnesium chloride hexahydrate; HCl: hydrogen chloride; CaCl<sub>2</sub>: Calcium chloride; Na<sub>2</sub>SO<sub>4</sub>: sodium sulfate; Tris: tris(hydroxylmethyl) aminomethane.

(6 mm) on each tooth. Materials' composition is provided in Table 1.

A curing radiometer (Model Bluephase® meter, Ivoclar Vivadent AG) to monitor the output intensity, 1000 mW/cm<sup>2</sup> as minimal output intensity, was employed. Restorations were kept in a dark environment and immersed in simulated body fluid solution (SBFS) (24 h). Four subgroups (n = 4), based on the type of challenging method, were established: (1) 24 h in SBFS, (2) Load cycling assay, (3) Collagenase solution, and (4) Thermal cycling test. The displayed methodology applied to each subgroup was as it follows (Figure S1): (1) restored teeth stored in SBFS for 24 h; (2) load cycled with sine wave form (225 Nw, 259,200 cycles, 3 Hz) (S-MMT-250NB; Shimadzu, Tokyo, Japan), as in Sauro et al., 2009 [10]; (3) immersion of the treated specimens in collagenase solution; resin-dentin interfaces were examined after 1-month of immersion in a collagenase solution, as in Zhang et al., (2020) [43]. The aging solution of collagenase was obtained by dissolving collagenase of Clostridium histolyticum (Sigma-Aldrich, St.Louis, MO, USA) into artificial saliva (20 mM HEPES buffer, 30 mM KCl, 4.0 mM KH<sub>2</sub>PO<sub>4</sub>, 0.2 mM MgCl<sub>2</sub>·6 H<sub>2</sub>O, 0.7 mM CaCl<sub>2</sub>,0.3 mM NaN<sub>3</sub>, pH 7.4 [44] to achieve a concentration at 0.1 mg/mL, protected from light and at 37°C. To avoid bacterial contamination, the collagenase solution was carefully removed and a fresh one was reapplied every 48 h; (4) thermal cycling test, specimens were subjected to thermocycling (100,000 cycles between 5°C and 55°C) (Thermocycler THE-1100, SD Mechatronik GmbH, Germany) in distilled water, for 3 months, with the specimens periodically submerged in each thermal bath for 30 s dwell time, with 10 s at air temperature between submersions to reproduce temperature alterations that can take place in the oral cavity.

## 2.3. Specimens' preparation for microtensile bond strength (MTBS) and field emission scanning microscopy (FESEM)

A slow-speed diamond saw (Accutom 50, Struers GmbH, Copenhagen, Denmark) was used to vertically section, into 1 mm-thick slabs, the bonded teeth. One slab of each molar was utilized for nanoindentation testing. In order to provide approximately 10 sticks per tooth, the rest of each tooth were serially sliced into beams with a cross-section of 1 mm<sup>2</sup>. The prepared samples were aligned in a soft glue gel (Zapit, Dental Ventures of America, Corona, CA, USA) before the application of a hardener agent (spray) to cure. A modified Bencor Multi-T testing device was used to fix each beam. This equipment assessed the failure in tension (0.5 mm/min crosshead speed) by utilizing a universal testing machine (Instron 4411; Instron Corporation, Canton, MA, USA). The crosssectional area at the failure site was measured by employing a set of 2 digital calipers (Sylvac Ultra-Call III, Fowler Co., Inc., Newton, MA, USA) (accuracy of 0.01 mm). Mean bond strength was expressed in MPa. The independent factors were the type of NPs (PTH-NPs, undoped NPs and control) and the procedure of challenging (24 h of storage, thermocycling and mechanical loading). ANOVA and Student-Newman-Keuls, (significance p < 0.05) for post hoc comparisons were employed. To analyze the failure mode of fractured samples (at 40  $\times$ magnification), a stereomicroscope (Olympus SZ-CTV; Olympus, Tokyo, Japan) was employed. Failure modes were registered as adhesive, cohesive or mixed. Dentin surfaces were then fixed for 24 h in a 2.5 %glutaraldehyde solution in 0.1 mol/L sodium cacodylate buffer. To observe the samples with a field emission scanning electron microscope (FESEM Gemini, Carl Zeiss, Oberkochen, Germany), they were exposed to critical point drying (Leica EM CPD 300, Wien, Austria) and sputtercoated with carbon by means of a sputter-coating Nanotech Polaron-SEMPREP2 (Polaron Equipment Ltd., Watford, UK).

#### 2.4. Nanoindentation testing

Four slabs from each subgroup (one per tooth) were nanoindented by using a Hysitron Ti 950 nanoindenter (Hysitron, Minneapolis, MN). The nanoindenter (Berkovich, three-sided pyramidal) had a diamond indenter tip radius of around 20 nm. The nanoindenter was previously

calibrated (force setpoint, 5  $\mu N$ ). Along the interface of each slab, in different mesiodistal positions, three lines of indentation 15( $\pm 5$ )  $\mu m$  were performed. Four indentation were undertaken to register the nanohardness (Hi) values, from the hybrid layer to the underlying dentin. The distance intervals steps, between indentations (5  $\pm$  1  $\mu m$ ), was preserved. In hydrated conditions, a load of 4000 nN during 10 s was applied. Water evaporation was prevented by ethylene glycol application over the sample surface in each scanning period. A macro! NSize V2010.06.30 analysis (power of analysis 80 %, confidence level 95 %) was utilized for sample size calculation. Mean nanohardness was expressed in GPa. The independent factors were the type of NPs (PTH-NPs, undoped NPs and control) and the procedure of challenging (24 h of storage, thermocycling and mechanical loading). ANOVA and Student-Newman-Keuls, (significance p < 0.05) for post hoc comparisons were employed.

#### 2.5. Raman spectroscopy and cluster analysis

To analyze dentin interfaces, a dispersive Raman spectrometer/microscope (Horiba Scientific Xplora, Villeneuve d'Ascq, France) was employed. A spot size of approximately 0.5  $\mu m^2$ , that operates at 785 nm, was used to determine the Raman signal (100 mW power at the surface of the sample) from 400 to 1700 cm $^{-1}$  Raman wavenumber [45]. At the interface, chemical mappings were performed. Two areas of 30  $\times$  30 mm, for each specimen, at different locations were mapped by employing 1 mm spacing at X and Y axes. Each spectrum was assessed throughout 2 s acquisition time doing 2 accumulations. A K-means cluster analysis (KMC) was performed for each mapping, which includes a multivariate analysis tool (Isys, Horiba), in order to generate independent clusters by a statistical pattern. Hierarchical cluster analysis (HCA), to order different natural sets of components was used.

Ward's technique was employed to create clusters. Five principal components calculated the dendogram that corresponded, at the resindentin interface, with five different components (red, more mineralized dentin; yellow, adhesive; purple, hybrid layer; blue, bottom of hybrid layer; green, dentin). All spectra described for each cluster were averaged to obtain the mean cluster spectrum. Thus, Raman measurements were obtained respect to the relative presence of mineral, phosphate (961 cm<sup>-1</sup>) and carbonate (1070 cm<sup>-1</sup>) peaks, where the height of peaks were registered in absorbance units. The intensity of the phosphate peak was also determined by mapping (2D micro-Raman map of 961 cm<sup>-1</sup> intensities).

#### 2.6. Confocal microscopy evaluation (CLSM)

Six more teeth per group were used for this assessment. Previous to the bonding application, bond resin was doped with 0.05 wt% Rhodamine B (RhB:Sigma-Aldrich Chemie Gmbh, Riedstr, Germany) to analyze the resin diffusion and the hybrid layer morphology. After that, the samples were divided in two halves, and each half was randomly assigned to one of the two subgroups: 1) the pulpal chamber was filled with 1 wt% aqueous/ethanol fluorescein (Sigma-Aldrich Chemie Gmbh, Riedstr, Germany) for 3 h (to analyze porosity, nanoleakage and micropermeability), and 2) teeth were immersed in 0.5 wt% xylenol orange solution (XO: Sigma-Aldrich Chemie Gmbh, Riedstr, Germany), excited at 514 nm for 24 h, at 37 °C (pH 7.2), to determine the novo calcium deposits. Samples were copiously rinsed with water and treated in an ultrasonic water bath for 2 min. Afterwards, they were sectioned in resin-dentin slabs and polished using ascending grit SiC abrasive papers (#1200 to #4000) on a water-cooled polishing device (Buehler-MetaDi, Buehler Ltd. Lake Bluff, IL, USA). The specimen preparation was finished with a last ultrasonic cleaning (5 min). Analysis of bonded interfaces was accomplished by a dye-assisted confocal microscopy valuation, employing a confocal laser scanning microscope equipped with × 60 lenses (SP5 Leica, Heidelberg, Germany). Rhodamine reveals resin diffusion and hybrid layer morphology; it is excited using green light

(540 nm) and emits red in color (590 nm). Fluorescein discloses the interior of the dentinal tubules, it is activated by blue light (488–495 nm) and emits green/yellow (520 nm). Xylenol will show, colored in yellow, new calcium deposits. 0.5 wt% xylenol orange is a calcium-chelator fluorophore commonly used in bone remineralization studies [46]. Xylenol orange is fixed in newly formed tissues where it remains until removal of the bone [47]. CLSM images were then obtained. Micrographs representing the most common features of micropermeability observed along the bonded interfaces were selected and recorded. Figure S1 shows a flow chart that explains the confocal analysis employed in this methodology.

#### 3. Results

#### 3.1. Nanoparticles fabrication and characterization

Fig. 1 is displaying TEM images of NPs. Agglomerated NPs were not presented, and NPs showed a spherical shape.

Fig. 2 is showing the ATR-FTIR spectra of the undoped NPs and PTH-NPs (blue and green lines, respectively). The presence of 2-hydroxyethyl methacrylate in both nanoparticles is confirmed by the formation of a broad absorption band between 3662 and 3093 cm<sup>-1</sup> corresponding to the stretching vibration of the hydroxyl group (-OH) [48]. In addition, a common peak is observed at  $\sim$ 2922 cm<sup>-1</sup> related to the aliphatic (C-H) stretching vibrations of 2-hydroxyethyl methacrylate and methacrylic acid compounds [48,49]. Another characteristic peak of 2-hydroxyethyl methacrylate is also present at 1724 cm<sup>-1</sup>, corresponding to the stretching vibrations of the carbonyl group (C=O) [48]. The methacrylic acid showed typical peaks at  $\sim 1438 \text{ cm}^{-1}$  (CH<sub>3</sub> - asymmetric bending)  $\sim 1391 \text{ cm}^{-1}$  (CH<sub>3</sub>-symmetric bending), and  $\sim 1262 \text{ cm}^{-1}$ (C-C-O stretching) [50]. The detection of ethylene glycol dimethacrylate was also confirmed in both nanoparticles by the formation of high-intensity peaks at 1144 cm<sup>-1</sup>, 955 cm<sup>-1</sup>, 862 cm<sup>-1</sup>, and 752 cm<sup>-1</sup> [51]. In the PHT nanoparticles spectra (green line) the presence of this peptide was confirmed by the appearance of a peak at 1540 cm<sup>-1</sup> (Amide I band) (pointer) and the formation of a shoulder in peak  $1712~\text{cm}^{-1}$  due to the overlap of the peak  $1633~\text{cm}^{-1}$  (pointer) which is characteristic of the PTH [52,53].

# 3.2. Microtensile bond strength results, mechanical, chemical and thermal degradation assessments

In general, samples submitted to collagenase immersion attained the lowest MTBS values, in the control group, but no significant differences were encountered if compared to the thermocycled samples (p > 0.05) (Table 2). When dentin samples were infiltrated with undoped NPs, specimens stored for 24 h and those submitted to mechanical loading showed the highest MTBS values (Table 2). When PTH-NPs were utilized to infiltrate demineralized dentin, the highest MTBS values were achieved after mechanical cycling, and the lowest values appeared in samples stored for 24 h and those submitted to thermocycling (p < 0.05) (Table 2). When considering specimens infiltrated with PTH-NPs, load cycled specimens or those submitted to collagenase immersion, showed the highest MTBS values (p < 0.05) (Table 2).

In all experimental groups, failures were mainly mixed. The lowest percentage of adhesive failures was attained when PTH-NPs were used (Fig. 3).

#### 3.3. Nanoindentation testing

Within the control group, samples submitted to load cycling attained higher Hi values than the rest of the samples, at the hybrid layer, bottom of hybrid layer and intact dentin (p < 0.05) (Fig. 4). When undoped NPs were used to infiltrate the conditioned dentin, load cycling increased Hi at the hybrid layer and at the bottom of the hybrid layer, when compared with the rest of the specimens (p < 0.05) (Fig. 4). Samples

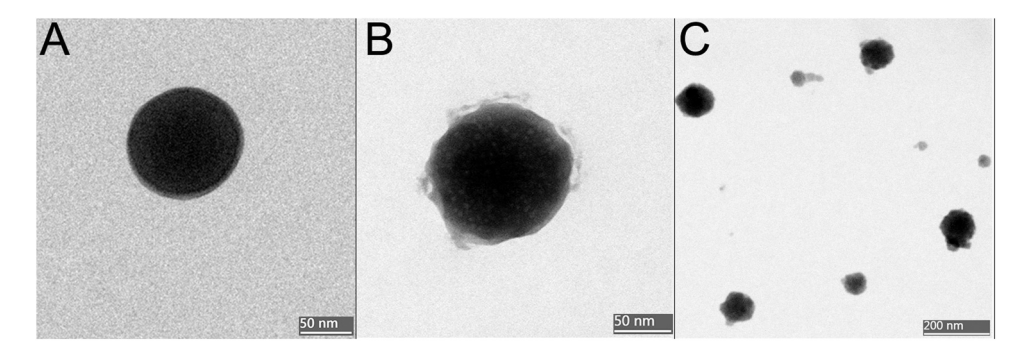


Fig. 1. Transmission electron microscopy (TEM) images of an undoped nanoparticle (undoped NP) (A), a PTH-doped NP (PTH-NP) (B) and a series of PTH-doped NPs (PTH-NPs) (C), showing no agglomeration. Light and dark objects inside the NPs corresponded with artifacts that developed during the transmission of the electron beam. Scale bars are 50 nm in (A) and (B), and 200 nm in (C).

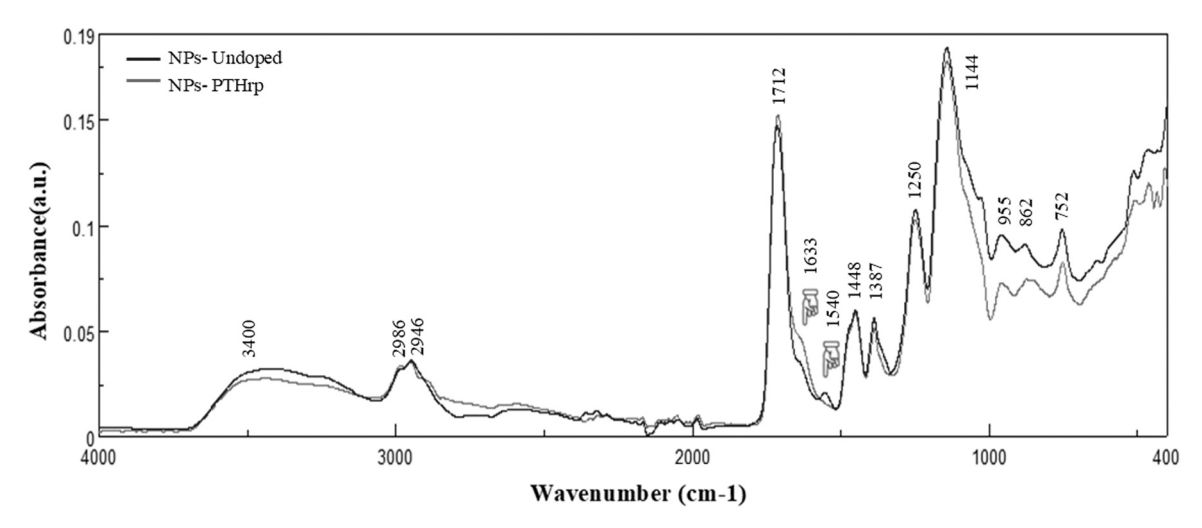


Fig. 2. Representative ATR-FTIR spectra of the experimental groups, undoped NPs and PTH-NPs. The figures also report the Peak Picking with both positions and intensities. Z potential was -12.7 mV for undoped NPs and -37.5 mV for PTH-NPs.

Table 2
Mean and standard deviation (SD) of microtensile bond strength (MTBS) (MPa) to dentin in the different tested groups sorted by challenges (24 h in SBFS -Control-, after load cycling, after 1 month in *collagenase* solution and after thermocycling).

Dentin Treatment	Mean (SD)	Mean (SD)					
	24 h	Load cycled	Collagenase (1 m)	Thermocycled			
Control	19.03 (3.12) a1	19.41 (3.13) a1	12.58 (2.48) a2	15.11 (4.66) a12			
Undoped NPs	15.52 (2.04) a12	19.57 (2.36) a2	12.91 (3.22) a1	12.90 (2.91) a1			
PTH-NPs	18.39 (2.89) a12	25.35 (2.75) b3	20.71 (3.62) b23	13.57 (2.58) a1			

Abbreviations: MTBS, microtensile bond strength to dentin; NPs, nanoparticles; PTH, Parathyroid hormone; SBFS, simulated body fluid solution; SD, standard deviations.

At vertical columns, same letter indicates no significant differences between treatment groups within the same challenging. At each row, same number indicates no significant differences between the storage method or challenge (24 h SBFS, load cycling, chemical aging for 1 month - collagenase- and 100,000 cycles thermocycled) in the same treatment group (p > 0.05).

treated with PTH-NPs showed the lowest Hi, at the HL, when they were stored for 24 h. At the HL and BHL, the highest Hi values were achieved by specimens submitted to load cycling (p < 0.05) (Fig. 4). Within the control group, specimens stored for 24 h and those submitted to thermocycling attained the lowest Hi throughout the whole resin-dentin interface, when compared with the load cycled samples (p < 0.05) (Fig. 4). When specimens were mechanically loaded, at the HL and at the BHL, samples infiltrated with PTH-NPs achieved the highest Hi. When specimens were thermocycled, at the HL, BHL and underlying dentin, samples infiltrated with PTH-NPs achieved lower Hi than samples mechanically loaded (p < 0.05) (Fig. 4).

### 3.4. Field Emission Scanning Electron Microscopy (FESEM)

Dentin specimens treated with PTH-NPs and load cycled showed a thicker layer of precipitates covering both the peritubular and intertubular dentin, forming a consistent clump of apparent crystals (Figs. 5A, 5B) mixed with the collagen fibers. The collagen fibers, at both peritubular and intertubular dentin, were not degraded neither collapsed. They showed a turgid appearance, and they seemed to be remineralized. Reinforced collagen could be observed after immersing in collagenase those dentin specimens which were infiltrated with PTH-NPs (Figs. 5C, 5D).

Specimens without NPs (control group), after load cycling, exhibited

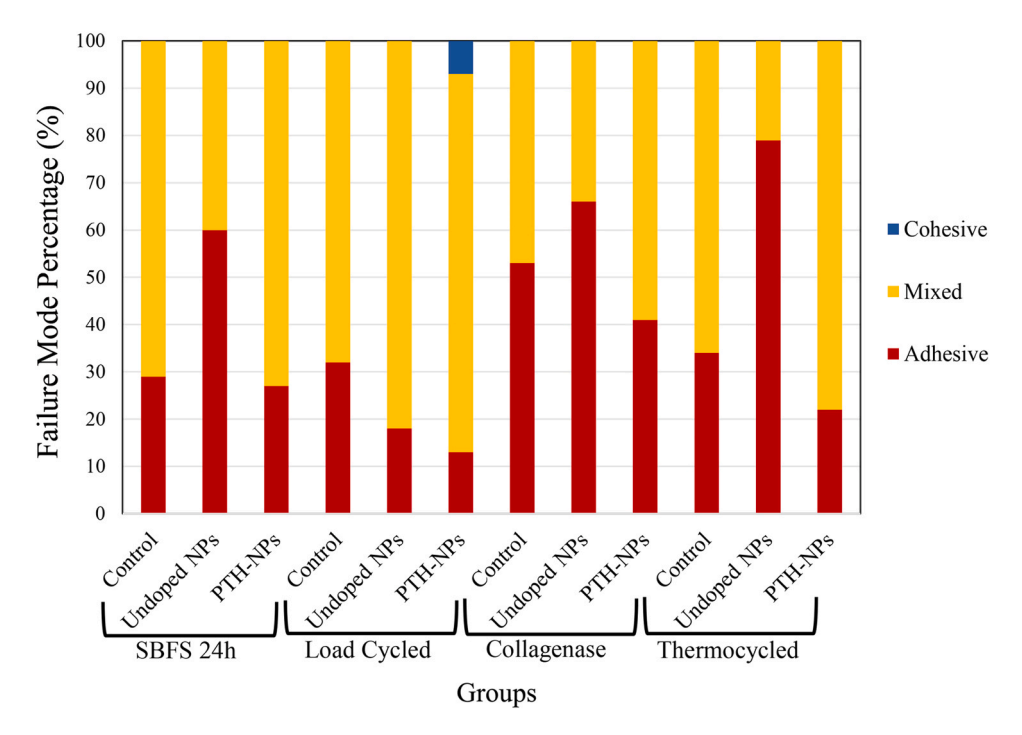
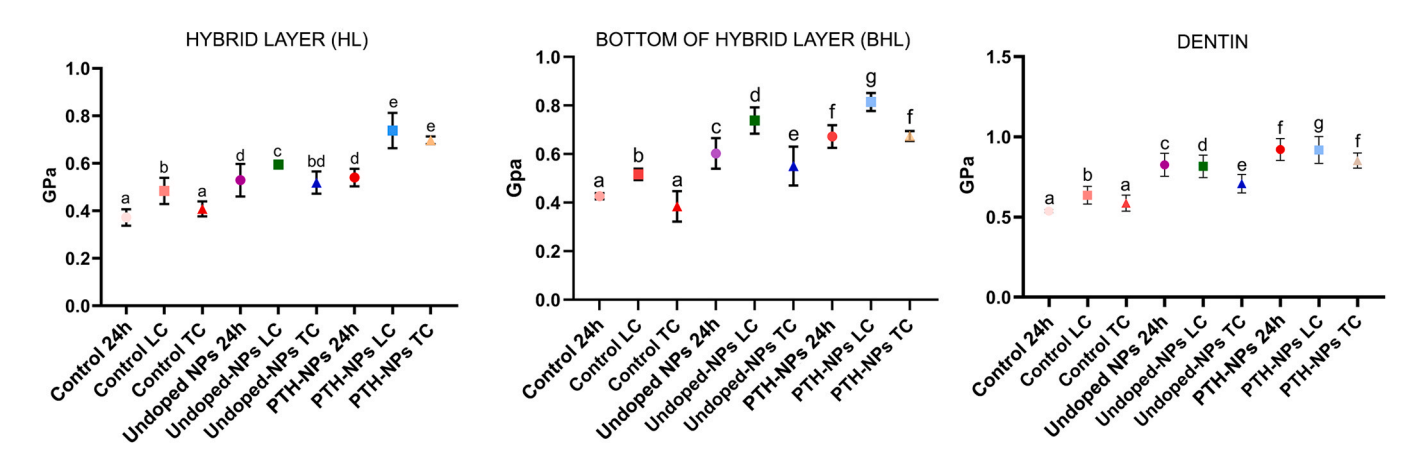


Fig. 3. Percentage distribution of failure mode of fractured specimens for the different tested groups. Abbreviations: PTH, Parathyroid hormone; NPs, Nanoparticles; SBFS, Simulated body fluid solution.



**Fig. 4.** Mean and standard deviation (SD) values of nanohardness (Hi) (GPa) in the different tested groups sorted by challenges (24 h in SBFS -Control-, load cycling and thermocycling) at the different zones of the bonded interfaces (hybrid layer, bottom of the hybrid layer and underlying dentin). Identical lowercase letter means no significant difference among distinct NPs at the experimental interfaces. Student-Newman-Keuls (p < 0.05) was used for *post hoc* comparisons. Abbreviations: BHL, bottom of the hybrid layer; HL, hybrid layer; NPs, nanoparticles; PTH, parathyroid hormone, LC, load cycled; TC, thermocycled.

a resin/collagen scaffold-like structure made of demineralized collagen, resin-infiltrated collagen and minerals (Fig. 6A). After immersing control specimens in collagenase, the failure occurred at the bottom of the hybrid layer, where multiple enlarged tubules and scarce resin tags were observed (Fig. 6B). Collagenase derived from Clostridium histolyticum can damage collagen chains and prompt collagen fibrils degradation. In vitro aging test was conducted in the bacterial collagenase solution storage to challenge dentin-adhesive bonds [43]. Undoped NPs infiltrated in conditioned dentin, and then load cycled, evidenced extensive areas of resin-dentin infiltration and provoked in strata apparent mineral precipitation, narrowing the entrance of tubules (Fig. 6C). Immersion, in collagenase solution, of dentin samples infiltrated with undoped NPs permitted to see an advanced degradation front at the bottom of the hybrid layer, where residual minerals, non-adapted resin tags and multiple NPs could be observed (Fig. 6D).

A generalized adhesive failure was observed in all specimens

analyzed after 24 h of storage. In these samples, hermetic sealing of tubules was not found (Figures S2A, S2E, S2I). Thermal cycling facilitated apparent mineralization of the dentin surface in control samples (Figure S2C) and in those treated with undoped NPs (Figure S2G). In both groups, absence of tags or imperfect sealing of tubules were characteristic. Specimens infiltrated with PTH-NPs and submitted to thermal cycling showed dentin reinforcement with robust resin tags and multiple traces of detached NPs (Figure S2K).

#### 3.5. Raman spectroscopy and cluster analysis

Concerning the analysis of the relative presence of minerals, specimens treated with PTH-NPs attained the highest phosphate and carbonate peaks, throughout the total resin-dentin interface at both 24 h storage and after mechanical loading, when compared with the rest of the groups. Conditioned dentin infiltrated with PTH-NPs produced a rise

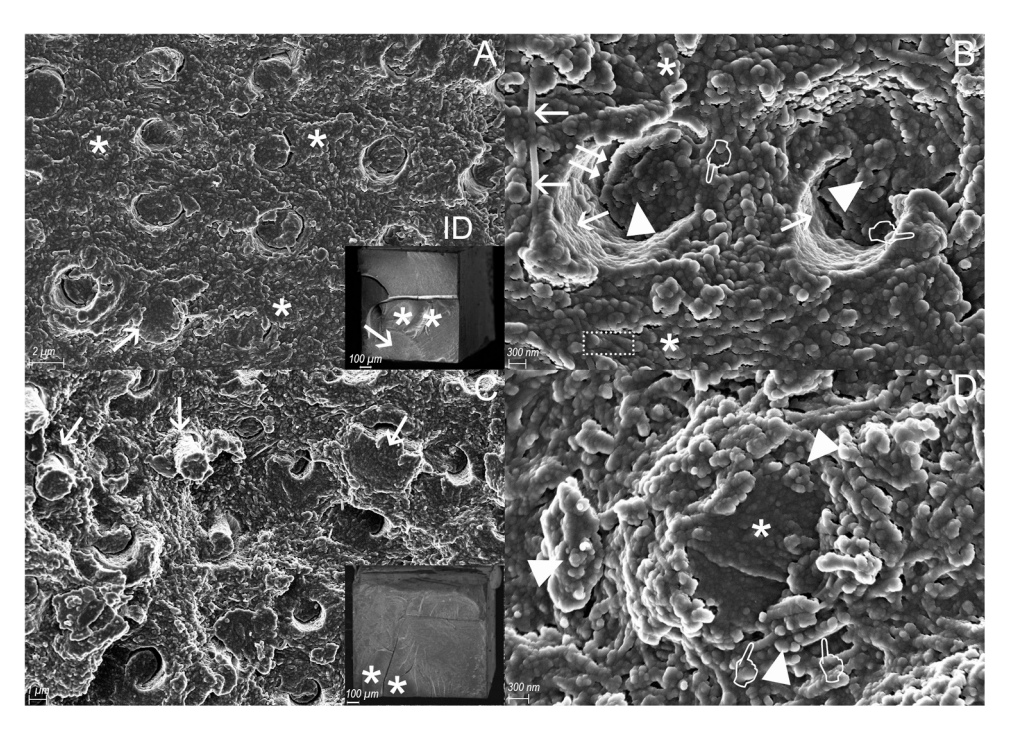


Fig. 5. A, FESEM observation of the debonded dentin surface when infiltrating PTH-NPs (PTH-NPs group) after load cycling and SBFS immersion. A material deposition, patterned in strata (asterisks), specially, at intertubular dentin (ID) was determined. Most of the tubules were closed (arrow). Inset: A mixed failure, and a fractured bottom of hybrid layer is seen (arrow). An adhesive resin layer remains at the middle of the picture (asterisks) (Scale bar: 100 μm). B, Same group than "A", but magnified. A collar of new deposits precipitated by the tubule lumen (pointers), and other new layered structures located below the former deposits (asterisk). Collagen fibers were found in the walls of tubules (arrows) or appeared isolated crossing over the intertubular dentin. Tags, with multiple incorporated NPs (arrowheads), and peritubular dentin (PD) unveiled occasionally imperfect bonding (double arrows). The peritubular wall permitted to observe multiple NPs, adhered to collagen fibers and to the tubule wall. D-periodicity banding (67 nm) of some collagen fibrils were seen (dotted rectangle). Tubules appeared filled (arrowheads). C, Sample treated with PTH-NPs after immersion in collagenase, 1 month. The fracture appears at the bottom of the hybrid layer. Tags partially occluded some tubules (arrows). Inset: A mixed failure, at the bottom of the hybrid layer, may be seen (asterisks) (Scale bar: 100 μm). D, Same group than "C", but magnified. NPs adhered to the collagen were observed on the tubular walls (pointers). The main tubule appeared with the lumen completely occluded (asterisk). Surrounding the rest of the tubule entrance, net-precipitated crystals covered part of the peritubular dentin. Enlarged NPs and mineral precipitation on dentin were adverted (arrowheads) (Scale bar: 300 nm). Abbreviations: PTH, Parathyroid hormone; NPs, nanoparticles.

of both carbonate and phosphate peaks after mechanical loading, at the bottom of the hybrid layer and intact dentin, in comparison with specimens 24 h storage. Thermocycled samples presented the lowest phosphate and carbonate peaks among groups (Table 3).

Substrata treated with PTH-NPs, after mechanical loading, achieved the highest phosphate peak intensity among groups (Fig. 7F).

#### 3.6. Confocal microscopy evaluation (CLSM)

Micropermeability, nanoleakage and porosity, at the resin-dentin interface, were present in the absence of NPs (control group) (Figure S2B), less accentuated when undoped NPs were infiltrated at the dentin (Figure S2F), after 24 h storage. PTH-NPs infiltration favored mineral precipitation at the resin-dentin interface, at 24 h. This was revealed after observing the strong signals of xylenol orange stain at the bonded interface (Figure S2J). An extensive micropermeability, porosity and nanoleakage were discovered after treating the conditioned dentin with Single Bond (control group) and load cycling (Fig. 8A·I).

Imaging for rhodamine (Fig. 8A·II), fluorescein (Fig. 8A·III) and reflected light channel (Fig. 8A·IV) were also exhibited. At the control group, both porous hybrid layer and adhesive layer resulted totally infiltrated by fluorescein (nanoleakage), after mechanical loading evaluation (Fig. 8A·II, 8 A·III). Micropermeability diminished after incorporating undoped NPs into the adhesive composition and applying load cycling (Fig. 8B·I). Imaging for rhodamine (Fig. 8B·II), fluorescein (Fig. 8B·III) and reflected light channel (Fig. 8B·IV) were also shown. At a whole, the CLSM analysis demonstrated that that resin-dentin interfaces of the control (Single Bond) (Fig. 8A·I) and undoped NPs

(Fig. 8B·I) load cycled samples attained deficient resin-hybridization. Both porosity and nanoleakage decreased (Figs. 8C, 8D·I), and mineralization augmented (Fig. 8D·II) at the resin-dentin interface, after infiltrating dentin with PTH-NPs and applying mechanical loading, when compared with the rest of the groups. Nanoleakage and porosity diminished after using undoped NPs (Fig. 8B·II, 8B·III), and much more after PTH-NPs resin-dentin infiltration and load cycling in both groups (Fig. 8C·II, 8 C·III). The fluorescent calcium-chelator dye xylenol orange was disclosed at the resin-dentin interface after infiltrating PTH-NPs and load cycling. Solid signals of xylenol orange presence were revealed within the dentinal tubules and at the top of resin-dentin interface (Fig. 8D·II).

CLSM and xylenol orange (Xo) images corresponding to the control group submitted to thermocycling exhibited faint micropermeability (Figure S2D·I) and new mineral deposition at both dentin tubules wall and the hybrid layer (Figure S2D·II). Dentin infiltrated with undoped NPs showed a clear pattern of micropermeability (Figure S2H·I), in spite of new mineral deposits along the dentinal tubules and within the hybrid layer (Figure S2H·II). Infiltration of PTH-NPs in conditioned dentin and then thermocycled permitted to observe, after xylenol orange application, strong mineral processes inside the dentinal tubules and at the hybrid layer (Figure S2L).

#### 4. Discussion

Conditioned dentin surfaces infiltrated with nanoparticles doped with parathyroid hormone (PTH-NPs) achieved the highest bond strength (MTBS) in any group of study, though significant differences

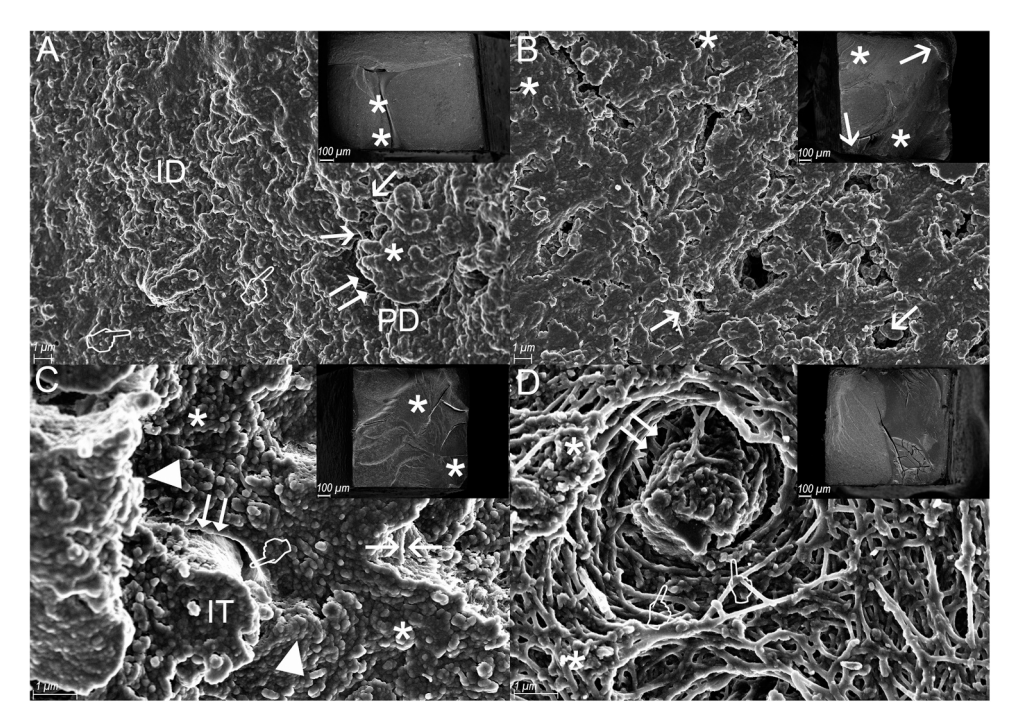


Fig. 6. A, FESEM images of the debonded dentin surface using Single Bond (Control) and load cycling at immersion of 24 h. Collagen fibers were hardly observed at intertubular dentin (ID), and scarcely distinguished at peritubular dentin (PD) (arrows). Some of them remained at the entrance of the tubules (asterisk). Precipitates were adverted (pointers). Partially sealed tubule entrances were observed (double arrows) (Scale bar: 1 μm). Inset: Fractured bottom of hybrid layer is seen (asterisks). B, FESEM observations of the same group after collagenase immersion (1 month). Collagen degradation may be observed underlying dentin. Some resin tags partially occlude the tubules (arrows), and protruding at the interface. (Scale bar: 1 μm). Inset: A generalized mixed failure is shown. Some scratches from the dentin preparation were detected (asterisks). Other areas revealed the presence of adhesive layer (arrows) (Scale bar: 100 μm). C, FESEM observations of the debonded surface treated with undoped NPs and load cycled after 24 h SBFS immersion. Areas of resin infiltration were detected (asterisks). Non adjusted resin tags against the tubules were seen (pointers). A collar of precipitates characterized the entrance of the tubule lumen (double arrows). Peritubular, intertubular and intratubular (IT) dentin appeared remineralized. Some demineralized collagen fibers were adverted (faced arrows) (Scale bar: 1 μm). Inset: Residual adhesive resin appears (asterisks) at distinct locations (Scale bar: 100 μm). D, FESEM observations of the debonded surface bonded with undoped NPs and immersion in collagenase (1 month). Agglomerated NPs forming collars were detected (pointers). Peritubular dentin is not present after conditioning and collagenase immersion (double arrows). Blocks of enlarged NPs were unveiled (asterisks) (Scale bar: 100 μm).

**Table 3**Raman intensities of the main mineral components (phosphate and carbonate peaks) attained from experimental interfaces after the proposal challenges.

		Phosphate [961 cm <sup>-1</sup> ]			Carbonate [1070 cm <sup>-1</sup> ]		
		24 h	LC	TC	24 h	LC	TC
Control	HL	46.64	70.89	50.45	10.01	9.15	7.98
	BHL	89.62	99.02	101.17	11.19	12.58	12.49
	Den	96.25	118.66	108.99	12.11	15.71	13.76
	2						
	Den	122.33	143.56	132.05	15.44	18.78	16.95
	1						
Undoped	HL	28.81	22.87	60.64	5.01	3.16	9.19
NPs	BHL	57.10	39.97	70.05	7.12	5.92	10.36
	Den	79.95	74.76	103.96	9.40	9.72	14.29
	2						
	Den	147.43	114.82	127.37	20.43	14.72	17.02
	1						
PTH-NPs	HL	174.61	116.67	45.91	20.56	20.33	8.71
	BHL	244.20	330.45	95.98	28.28	43.97	14.53
	Den	357.52	438.90	122.00	42.84	57.48	17.23
	2						
	Den	524.83	529.37	147.43	62.23	71.48	20.43
	1						

Abbreviations: NPs: nanoparticles; PTH: Parathyroid hormone; HL: Hybrid layer; BHL: Bottom of hybrid layer; Den 2: second point of testing at dentin; Den 1: first point of testing at dentin; LC: 24 h load cycling; TC: 100000 thermal cycles. The peaks values had been normalized to the basis of the carbon–carbon aromatic vibration band at  $1608~\rm cm^{-1}$  (near  $1600~\rm cm^{-1}$ ). Peaks positions are expressed in cm $^{-1}$ .

were only attained in the groups submitted to immersion in collagenase solution or to load cycling (Table 2). These findings become associated to a gain in mineralization (observed at the Raman analysis), correlated to augmented precipitation of minerals at the demineralized collagen (FESEM observations) and to an advanced functional remineralization at the hybrid layer and at the bottom of the hybrid layer (nanoindentation). As a consequence, both porosity (indicative of demineralization and /or insufficient resin infiltration) and nanoleakage (leakage of fluorescein through the demineralized dentin denoting micropermeability) decreased after PTH-NPs infiltration at the resindentin interface, increasing the sealing ability [46]. The creation of mineralized interfaces, after mechanical loading or thermocycling were also favored, as porosity, micropermeability and nanoleakage diminished or disappeared in specific zones of the resin-dentin interface. It has been stated that porosity within the hybrid layer is also the result of unpolymerized monomers that leach out and hydrolysis or degradation of collagen, among others [54]. Porosity, in confocal microscopy evaluation (CLSM), indicates demineralization and /or insufficient resin infiltration throughout the conditioned dentin. The existence of porosity, at the resin dentin interface, is revealed by the presence of fluorophores (fluorescein) (green dye) previously placed in the pulp chamber, which determines micropermeability [55], regulating the sealing ability of the hybrid layer. The presence of a bioactive material at the interface generates dentin biomineralization. The new mineral refills the original pores provoked by the demineralization, diminishing the green emission. The clinical significance of these findings correlates with the formation of mineral precipitants within the interface, which seal both the porosity of the hybrid layer and the non-hybridized resin

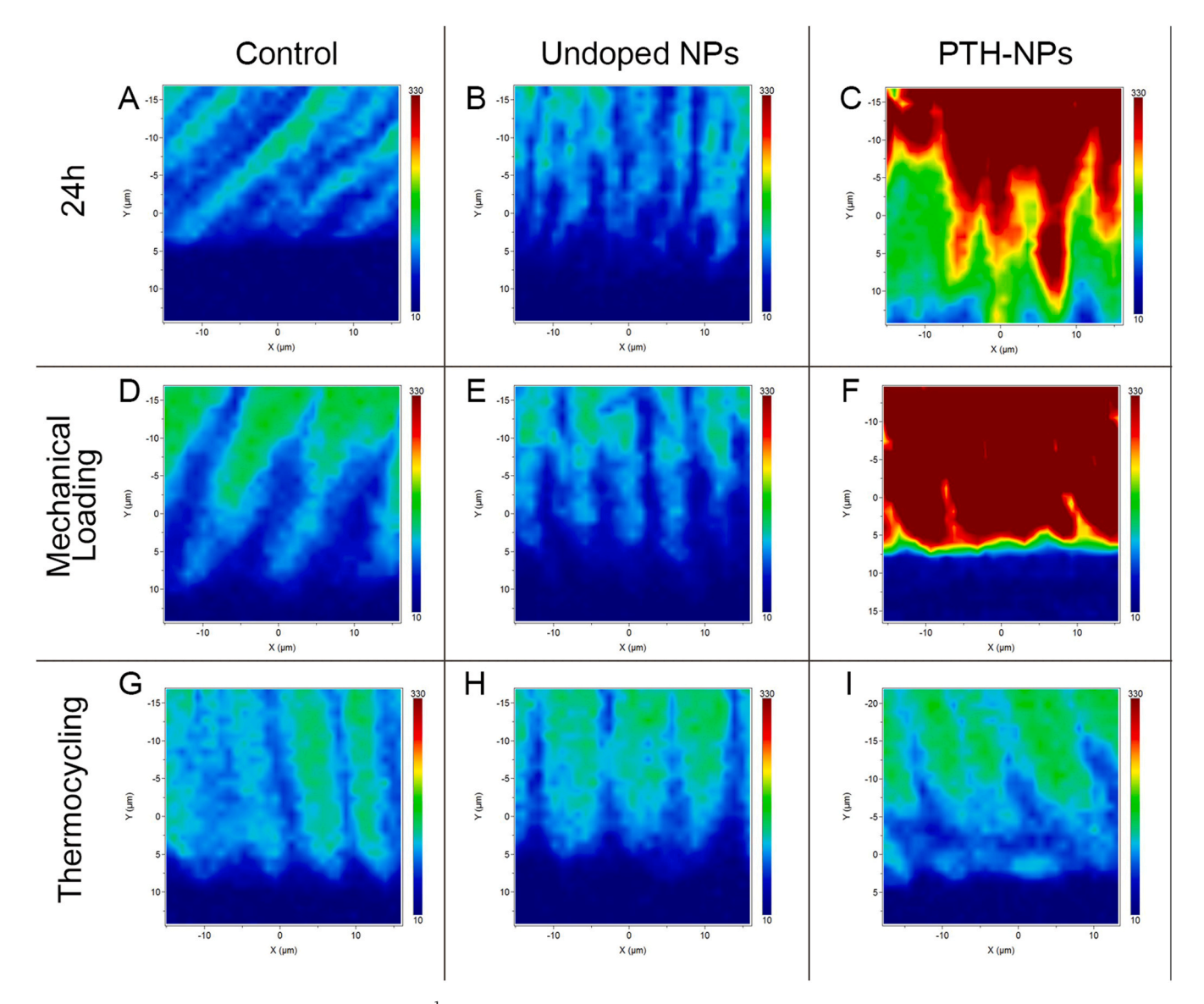


**Fig. 7.** Raman analysis [2D micro-Raman map of 961 cm<sup>-1</sup> intensities] of the dentin interfaces analyzed at 24 h of storage: control (A), treated with undoped NPs (B) and parathyroid hormone (PTH)-doped NPs, PTH-NPs (C). Interfaces from the same groups when submitted to mechanical loading (D, E, F, respectively) and thermocycling (G, H, I, respectively). At the 2D micro-Raman, the red represents the highest peak intensity, while the blue represents the lowest.

tags [56]. On the other hand, the presence of the adhesive resin at the interface is denoted by the visualization of the color red from rhodamine. Dyes have been mixed with components for analysis of the distribution of resins through the resin-dentin interface, providing data about micromorphology [57]. Therefore, the first null hypothesis must be rejected at a whole. The lowest percentage of adhesive failures was verified by dentin interfaces infiltrated with PTH-NPs (Fig. 3), that indicated the existence of a solid attachment at the resin-dentin interface.

Hydrodynamic size distribution of nanoparticles was previously assessed by dynamic light scattering, and average size was probed to be the same before and after loading of NPs (250–225 nm) [58] with a polydispersity index (PDI) of  $0.02 \pm 0.0015$  [59]. It has to be mentioned that even when NPs are theoretically defined when they are within the range of 1–100 nm, it is currently accepted, following recommendations on biomaterials terminology that they are NPs whenever being below 500 nm [60,61]. Optimizing the durability and the integrity of the resin-dentin bond in demineralized dentin poses one of the pivotal challenges in restorative dentistry [7]. At 24 h storage, the dentin infiltration of peptides (PTH) has promoted mineral nucleation into the

interface [62], without contributing to any significant bond strength augmentation when compared with those resin-dentin interfaces infiltrated with undoped NPs (Table 2). The new deposited structure that was observed by FESEM (Figure S2I) and confirmed to be mineral (calcium and phosphate) by Raman analysis (Table 3) after PTH-NPs infiltration was in line with the signals of orange stain that were shown at the bottom of the hybrid layer, where resin is absent, and at the tubule walls that noticeably stained with the calcium chelator dye (Figure S2J). The phosphate peak characterizes the tetrahedral PO<sub>4</sub> group within the hydroxyapatite (HAp). The intensity peak can be monitored to assess the phosphate content [63] through 2D micro-Raman analysis. In the present research, the highest phosphate intensity was clearly determined in dentin substrate infiltrated with PTH-NPs mechanically loaded, as the area and intensity of the red color of the mapping was remarked among groups (Fig. 7F). When PTH-NPs specimens were subjected to load cycling, the corresponding HCA Raman results (centroids) showed an increase in the phosphate peak intensity (Fig. 7F), when compared with the undoped NPs treated samples (Fig. 7E), meaning mineral advance. Therefore, at 24 h dentin remineralization did occur. It has been evidenced that phosphoric acid

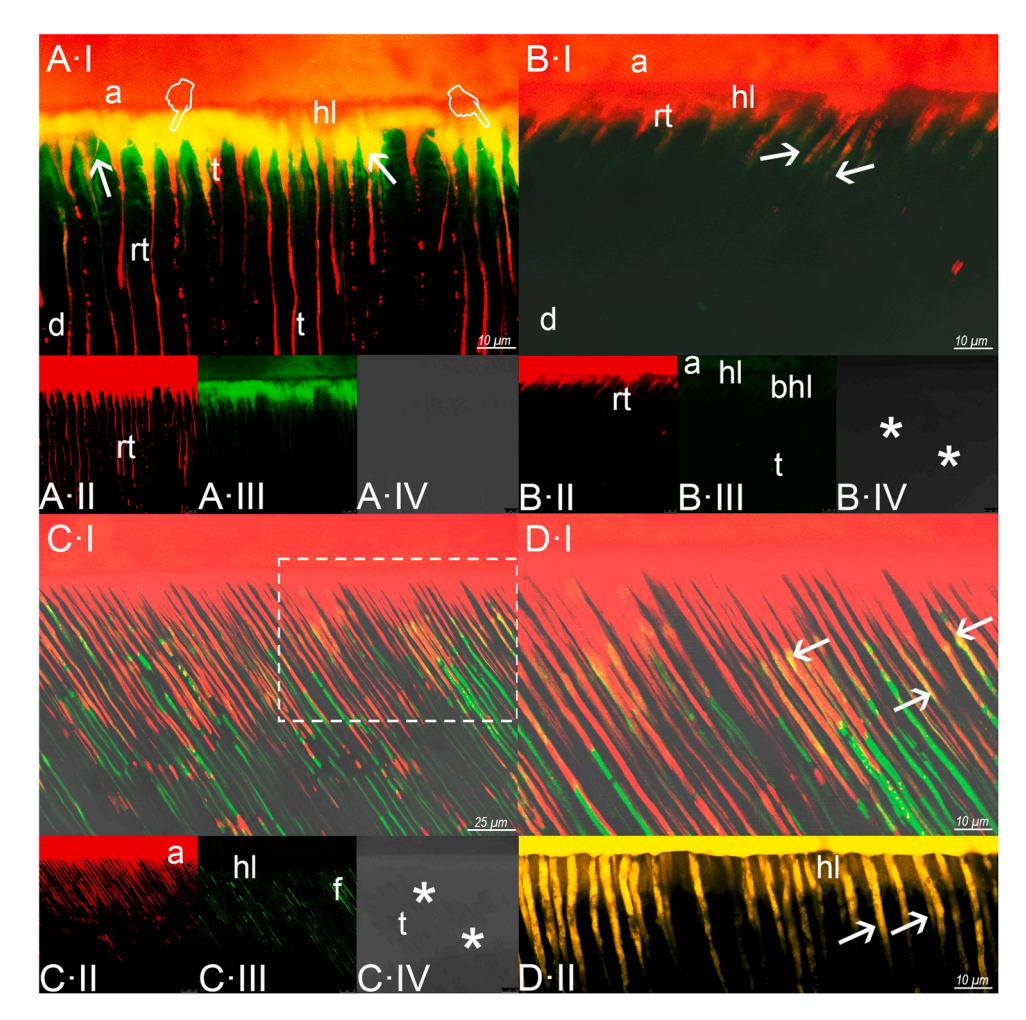


Fig. 8. CLSM of the created interfaces in reflexion/fluorescence mode, A-I: Control group, after mechanical loading. An extensive micropermeability pattern is shown (arrows). A strong nanoleakage signal is detected (pointers) at the hybrid layer (hl). A clear spectral overlap (yellow) of both dyes (red and green), is identified with determinant signs of nanoleakage. Funneling (f) of the tubular entrances is observed. A high dye sorption at the adhesive layer was noticed. Short and narrow resin tags (rt) with discontinuities were detected (Scale bar: 10 μm); A-II Red channel for rhodamine; A-III green channel for fluorescein; and A-IV correspond to the reflected light channel. a, adhesive layer; d, dentin; hl, hybrid layer; t, dentin tubules; rt, resin tags. B-I, Images corresponding to samples treated with undoped NPs and load cycling. Micropermeability between the adhesive (a) and the hybrid layer (hl), and within the dentinal tubules is observable (arrows) (Scale bar: 10 μm). B-II, Corresponds to the Figure B-I, but imaged in rhodamine only. Soft fluorescein water sorption characterized the B-III. Reflective signals appeared in B-IV (asterisks). a, adhesive layer; d, dentin; hl, hybrid layer; bl, bottom of hybrid layer; t, dentin tubules. C-I, Images corresponding to samples treated with PTH-NPs and load cycling. No signs of nanoleakage are seen, generally (Scale bar: 25 μm). In fluorescence mode, with rhodamine, many varied resin tags (rt), (C-II) were observed. In fluorescein mode (C-III), a profuse dye sorption at the adhesive layer was noticed. Limited reflective signals, in C-IV, were detected at the dentinal tubules (t). a, adhesive layer; f, funneling; hl, hybrid layer; t, dentinal tubules. D-I, Images corresponding to samples treated with PTH-NPs and load cycling. The dotted square in C-I, magnified, indicates Fig. 8D (Scale bar: 10 μm). A mild spectral overlap (yellow) of both dyes (red and green), relates with a brief sign of nanoleakage (arrows) (Scale bar: 10 μm). D-II, PTH-NPs and load cycling e

demineralized dentin is a bioactive matrix, being able to form HAp onto the surface as early as 30 min [64]. The existence of enzymes and remineralizing factors within the dentin matrix may have facilitated remineralization under favorable conditions [65]. A satisfactory surface nucleation of apatite may cause a faster deposition of Ca-P minerals on the surface of demineralized dentin [66]. Once surface crystallization takes place, the mineral precursors may have been likely sequestered by existing crystallites and thus precipitate, as suggested by HRSEM [64]. The presence of this nucleating surface induces structural and compositional changes that enable the denser packing of the clusters and their subsequent fusion to form amorphous calcium phosphate and ultimately apatite crystals [67,68]. Kim et al. (2011) [69] have established that to promote a growth centre, collagen structure should be sound in addition to the presence of residual mineral crystals. The mineral-inductive capacity of partially demineralized dentin may be explained, in addition, by the presence of insoluble phosphoproteins, in decalcified collagen,

serving as a locus for nucleation for mineral and so enabling the remineralization to occur, in vitro, starting at intertubular dentin [70]. Calcium is a crucial ion for mineralization [71]. The pivotal role of PTH in the mineralization was indirectly indicated through the increased formation of mineralized nodules, as calcium nodule precipitation is indicative of mineralization [72] of the dentin substrate. Nevertheless, after dentin infiltration with the self-assembling peptide P11-4, de Sousa et al. [73] obtained significant differences in bond strength evaluation, underscoring the critical role of the specific binding-site zone of collagen in its structure. Distinct ligands which are present in peptides such as carboxamide, hydroxyl or carboxyl groups may bind to calcium [74], triggering further nucleation. In the present research, the presence of PTH has been confirmed by ATR-FTIR analysis (Fig. 2), as the appearance of a peak at 1540 cm<sup>-1</sup> (Amide I band) and the formation of a shoulder in peak 1712 cm<sup>-1</sup> due to the overlap of the peak 1633 cm<sup>-1</sup>, are characteristic of the parathyroid hormone [52,53].

Concerning the molecular mechanism implicated in PTHrP-mediated mineralization, little is known. The reparative dentin formation has been demonstrated to be accelerated by PTH (1–34) [26]. PTHrP is a peptide that forms part of the parathyroid hormone family. Its specific C-terminal domain induces osteogenic features. Intracellular Ca<sup>2+</sup> is stimulated by C-Terminal PTHrP through a receptor different from the Type 1 PTH/PTHrP [75]. It seems that in the 1–34 N-terminal domain, osteostatin (OST), of this fragment, resides its biological activity [72, 76]. OST has also encouraged odontogenic differentiation, as probed by mineralized nodules formation [22,77]. OST increases phosphorylation [76], and exerts a bone anabolic activity. However, in order to specify the type of interaction that PTH does exert with the dentin structure, more research is required.

Challenging the resin-dentin interface can be investigated by applying load cycling test, submitting the tested samples to thermal stress, of chemically challenging the resin dentin interfaces with collagenase immersion [10,78]. Ideally, dental restorations should mechanically perform as dental structures during oral function. After using PTH-NPs, load cycling has significantly increased bonding efficacy (Table 2). At all mineralization sites, intermittent load triggers the activity of alkaline phosphatase, which is a zinc-metalloenzyme that protects collagen [79] generating free phosphate after hydrolysis, leading to apatite supersaturation [80]. This cascade orchestrates the amorphous calcium phosphate penetration that coalesces into collagen [7], lastly promoting hierarchical mineralization [81]. An association between resistance of collagen to enzymatic degradation and load cycling has also been established [82]. Thereby, mechanical loading has favored the precipitation of mineral deposits at the resin dentin interface diminishing porosity and nanoleakage, favoring the sealing of the interface [83], at the expenses of mineral deposition at the whole resin-dentin interface [84,85] infiltrated with PTH-NPs (Figs. 8C, 8D) (Table 3). Both mechano-sensitive and voltage-sensitive Ca<sup>2+</sup> channels might have influenced the mechanistics regulation of the formation of PTH-induced new minerals [26]. FESEM analysis showed new material deposits, or mineral precipitation [46] reinforcing both peritubular and intertubular dentin, appearing as collars around the lumen of tubules or forming multiple layers of new materials, tentatively minerals, in strata, respectively (Fig. 5A). Nevertheless, these images exposed, in some locations, the lack of hermetic tags sealing (Fig. 5B), that might have conditioned the presence of some yellow traces in the test of confocal microscopy (Fig. 8D·I). After multi-fluorescence examination, the Rhodamine B-labeled hybrid layer and an adhesive layer completely labeled by fluorescein penetration (nanoleakage) through the porous resin-dentin interface may be observed. Both were imaged at the same time by combining specific filters after matching the excitation line and the emission band. This technique permits assessing specimens that contain two fluorophores labeling different targets, observing each target separately, or at the same time. The advantage of simultaneous excitation is that the corresponding pixels of the two images are definitely in register because a single spot of incident light is the source for both [86], allowing overlap between both original channels. As a result, a clear spectral overlap (yellow) of both dyes (red and green) between the demineralized collagen and the infiltrated resin is identified with determinant signs of nanoleakage and further degradation [87]. The increase of the relative presence of minerals (Table 3) and the precipitation of minerals at the previous demineralized dentin has contributed to the protection of the exposed collagen. Collagen protection, after remineralization (Figs. 5, 8C), has been added to the increase in nanohardness, even though the adhesive polymer chain did not fully entrap the total collagen substrate [7] (Fig. 8D·I, 8D·II). The lesser degradation of collagen correlates with the greater mineralization [7]. On the contrary, after undoped NPs application and load cycling, relative or partial dentin mineralization has been proved in the present research, as some non-adapted resin tags, demineralized collagen fibers and empty dentinal tubules were unveiled (Fig. 6C). As a result, the bonding efficacy of dentin interfaces promoted with undoped NPs resulted

compromised in comparison with those treated with PTH-NPs and load cycled, as bond strength diminished in absence of PTH (Table 2). Confocal microscopy confirmed the presence of a discrete micropermeability at the resin dentin interface in spite of wide resin tags, that were not able to efficiently seal the dentin interface (Fig. 8B), when samples of conditioned dentin were infiltrated with undoped NPs and further submitted to the mechanical loading procedure.

Dentin infiltrated with PTH-NPs and immersed in collagenase, which exemplifies an accelerated model for degradation of the resin-dentin interface [88], achieved the highest MTBS values among different NPs groups (20.71 MPa), significantly different from the rest of specimens (Table 2). It is speculated that, in the resin-dentin interface, the existence of the NPs-carried hormone, as a peptide, may have augmented the collagen fiber stiffness within the dentin extracellular matrix, provoking higher resistance to proteolysis of collagen type I fibers [81]. FESEM images determined mineral precipitation and advanced mineralization, with dentinal tubules appearing mostly occluded after PTH-NPs infiltration, though other tubules were partially occupied (Figs. 5C, 5D). The presence of PTH at the interface made the bond strength decrease in the group of samples thermocycled in comparison with those which were load cycled (Table 2). Porosity and nanoleakage increased after applying PTH-NPs in dentin submitted to thermal cycling, where clear fluorescent-dye uptake (nanoleakage) was observed (data not shown), elucidating the degradation process. Funneling is considered an essential sign of degradation of the poorly resin-infiltrated demineralized peritubular dentin [46] as observed after evaluation of the fluorophore that labeled Rhodamine as a separate target. This advance degree of degradation may be attributed to the high hydrophilicity of this interface, which may have permitted excessive water adsorption and induced severe resin degradation as well as the extraction of water soluble unreacted monomers or oligomers from the resin matrix [89]. In demineralized resin-dentin interfaces, fluorescein (green) permeates through the zones which were infiltrated with rhodamine (red), then both colors overlapped providing a resultant yellow color that indicates nanoleakage [46]. Nevertheless, new minerals precipitated along the entire resin-dentin interface and at the dentin tubule walls (Figure S2L). FESEM examination permitted to observe dentin surface intensely restored after PTH-NPs infiltration and thermocycling. The adhesion between adhesive tags and peritubular dentin was not hermetic at all (Figure S2K). These gaps increased in case of dentin infiltrated with undoped NPs and thermocycling (Figure S2G).

Next, whether the presence of PTH at the resin-dentin interface had an effect in mineralization through nano-indentation assessment was examined. The obtained outcomes in the present study after PTH-NPs dentin infiltration may be understood as the consequence of a higher mineralization. In regenerated bone, PTH has also contributed to an increased hardness with accelerated bone remineralization [31]. A relative increase of Ca and P in peritubular dentin, associated to a microhardness rise has also been previously proved [19]. The highest Hi values at hybrid layer, bottom of hybrid layer (0.73 and 0.83 GPa, respectively), and even at the underlying dentin (Fig. 4), were attained at these interfaces infiltrated with PTH-NPs after load cycling, and are linked to a process of intrafibrillar mineralization of the collagen [7], low permeability, nanoleakage and porosity (Figs. 8C, 8D). This intrafibrillar apatite precipitation might "fossilize" matrix metallo-proteases and cathepsins, hindering their access to catalytic sites at collagen [7, 90]. As a result, the second null hypothesis must also be rejected. The advanced sealing ability that was proved became linked to the formation of HAp that would obliterate pores and voids. Intrafibrillar remineralization is commonly associated with mineral maturation and improved mechanical properties [91,92]. It can be speculated that PTH-NPs perform as analogs of non-collagenous phosphoproteins, serving as a template by binding to collagen, to induce formation of new mineral clusters and growth of apatite crystals in demineralized dentin [93]. In samples treated with undoped NPs and in control specimens, the Hi decrease at the hybrid layer (Fig. 4) correlates with dentin

demineralization and later degradation. This indicates scarce functional remineralization potential at the intrafibillar compartment [7] after load cycling, slowing down the active dentin remodeling capacity. A functional remineralization procedure only can be taken into account if the growth of the mechanical properties is achieved at the bonded interface [94]. Microleakage, micropermeability, structural porosity and demineralization-collagen degradation and are closely related [95,96]. Functional mineralization of collagen only happens when the fibrils of collagen are reinforced by minerals deposited at the intrafibrillar compartment. Only in these circumstances, the mechanical recovery of demineralized dentin is feasible [7]. As a result, we speculate that PTH may be considered as a potent biomimetic agent in the restoration of oral hard tissues. Further research to elucidate this point is required.

To the best of our knowledge, these are the only obtainable results from nano-indentation experiments with bond strength assessment, morphological and chemical characterization from dentin surfaces treated with PTH-doped NPs submitted to in vitro functional stresses. The proposed PTH-loaded NPs have demonstrated morphology, chemical, bonding properties and bioactive capacity to be utilized in dentin tissue engineering. PTH-NPs produce the strengthening of the dentin structure and a generalized occlusion of the tubules. Thereby, they should be recognized as a viable strategy to achieve dentin remineralization and sealing. This experiment gathers some limitations. X-ray micro-computed tomography analysis and X-ray fluorescence microscopy analysis should be realized, in order to incorporate morphophysico- chemical surfaces evaluation. Other limitation is translating this data to the clinical setting. Despite our best effort in simulating the oral environment by using SBFS storing, mechanical loading, collagenase and thermocycling, this is not a substitute for the true oral environment. This is another limitation of our study. The response to these PTH-NPs could be further considered as a potential therapy in diseases that usually compromise the dentin formation as dentinogenesis imperfect or X-linked hypophosphatemic rickets. Further complementary in vitro investigations on the osteogenic potential of PTH-NPs should be implemented.

#### 5. Conclusions

Nanoparticles doped with parathyroid hormone-related protein (PTHrP) endorsed the highest efficacy in dentin bonding, showing the utmost bond strength values, among groups after collagenase immersion and load cycling application, facilitating the formation of new mineral deposits throughout the resin-dentin interface. Mechanical loading stimulated dentin remineralization at the hybrid layer, bottom of hybrid layer and dentinal walls, and reduced permeability throughout the dentin-bonded interface. This remineralization was functional, linked to a process of intrafibrillar mineral nucleation, associated to an increase of both phosphate and carbonate. Dentin infiltrated with polymeric nanoparticles functionalized with PTHrP facilitated mineral precipitation, forming consistent clump of minerals at intertubular dentin and remineralizing collagen fibers at both peritubular and intertubular dentin. Mineral deposits were also located at the entrance of dentinal tubules, that provoked a narrowing of the tubuli lumen. The mineral precipitation associated to NPs doped with PTHrP dentin infiltration inducted lower nanoleakage and porosity, and better sealing when compared with the other groups, though not all dentinal tubules were hermetically sealed after remineralization with PTHrP.

### **Declaration of Competing Interest**

The authors declare that they have no known competing financial interests or personal relationships that could have appeared to influence the work reported in this paper.

#### Acknowledgments

The present study was supported by Grant PID2023-1516230B-I00 funded by MICIU/AEI/10.13039/501100011033 and by ERDF/EU. M. T.O. (P5A2024-92) and R.T. (P5A2024-93) hold Research Fellowships for Undergraduate Students from the University of Granada. Funding for open access charge: Universidad de Granada/CBUA.

The authors would like to thank Dr. Cifuentes-Jiménez for her assistance with the ATR-FTIR analysis.

#### Appendix A. Supporting information

Supplementary data associated with this article can be found in the online version at doi:10.1016/j.dental.2025.06.017.

#### References

- [1] Sordi MB, Fredel MC, da Cruz ACC, Sharpe PT, de Souza Magini R. Enhanced bone tissue regeneration with hydrogel-based scaffolds by embedding parathyroid hormone in mesoporous bioactive glass. Clin Oral Invest 2023;27:125–37. https:// doi.org/10.1007/s00784-022-04696-3.
- [2] Breschi L, Mazzoni A, Nato F, Carrilho M, Visintini E, Tjäderhane L, et al. Chlorhexidine stabilizes the adhesive interface: a 2-year in vitro study. Dent Mater 2010;26:320–5. https://doi.org/10.1016/j.dental.2009.11.153.
- [3] De Munck J, Van den Steen PE, Mine A, Van Landuyt KL, Poitevin A, Opdenakker G, et al. Inhibition of enzymatic degradation of adhesive-dentin interfaces. J Dent Res 2009;88:1101–6. https://doi.org/10.1177/ 0022034509346952
- [4] Spencer P, Ye Q, Park J, Topp EM, Misra A, Marangos O, et al. Adhesive/Dentin interface: the weak link in the composite restoration. Ann Biomed Eng 2010;38: 1989–2003. https://doi.org/10.1007/s10439-010-9969-6.
- [5] Breschi L, Mazzoni A, Ruggeri A, Cadenaro M, Di Lenarda R, De Stefano Dorigo E. Dental adhesion review: aging and stability of the bonded interface. Dent Mater 2008;24:90–101. https://doi.org/10.1016/j.dental.2007.02.009.
- [6] Pashley DH, Tay FR, Breschi L, Tjäderhane L, Carvalho RM, Carrilho M, et al. State of the art etch-and-rinse adhesives. Dent Mater 2011;27:1–16. https://doi.org/ 10.1016/j.dental.2010.10.016.
- [7] Moreira KM, Bertassoni LE, Davies RP, Joia F, Höfling JF, Nascimento FD, et al. Impact of biomineralization on resin/biomineralized dentin bond longevity in a minimally invasive approach: An "in vitro" 18-month follow-up. Dent Mater 2021; 37:e276–89. https://doi.org/10.1016/j.dental.2021.01.021.
- [8] Tjäderhane L, Nascimento FD, Breschi L, Mazzoni A, Tersariol ILS, Geraldeli S, et al. Optimizing dentin bond durability: control of collagen degradation by matrix metalloproteinases and cysteine cathepsins. Dent Mater 2013;29:116–35. https://doi.org/10.1016/j.dental.2012.08.004.
- [9] Monticelli F, Osorio R, Toledano M, Tay FR, Ferrari M. In vitro hydrolytic degradation of composite quartz fiber-post bonds created by hydrophilic silane couplings. Oper Dent 2006;31:728–33. https://doi.org/10.2341/05-151.
- [10] Sauro S, Mannocci F, Toledano M, Osorio R, Pashley DH, Watson TF. EDTA or H3PO4/NaOCl dentine treatments may increase hybrid layers' resistance to degradation: a microtensile bond strength and confocal-micropermeability study. J Dent 2009;37:279–88. https://doi.org/10.1016/j.jdent.2008.12.002.
- [11] Peters MC, Bresciani E, Barata TJE, Fagundes TC, Navarro RL, Navarro MFL, et al. In vivo dentin remineralization by calcium-phosphate cement. J Dent Res 2010;89: 286–91. https://doi.org/10.1177/0022034509360155.
- [12] Alaohali A, Salzlechner C, Zaugg LK, Suzano F, Martinez A, Gentleman E, et al. GSK3 Inhibitor-induced dentinogenesis using a hydrogel. J Dent Res 2022;101: 46–53. https://doi.org/10.1177/00220345211020652.
- [13] Medina-Castillo AL, Fernandez-Sanchez JF, Segura-Carretero A, Fernandez-Gutierrez A. Micrometer and submicrometer particles prepared by precipitation polymerization: thermodynamic model and experimental evidence of the relation between flory's parameter and particle size. Macromolecules 2010;43:5804–13. https://doi.org/10.1021/ma100841c.
- [14] Osorio MT, Toledano R, Huang H, Toledano-Osorio M, Osorio R, Huang C-YC, et al. Effect of doxycycline doped nanoparticles on osteogenic/cementogenic and antiinflammatory responses of human cells derived from the periodontal ligament. J Dent 2023;137. https://doi.org/10.1016/j.jdent.2023.104668.
- [15] Neves VCM, Babb R, Chandrasekaran D, Sharpe PT. Promotion of natural tooth repair by small molecule GSK3 antagonists. Sci Rep 2017;7:39654. https://doi.org/ 10.1038/srep39654.
- [16] Osorio R, Osorio E, Medina-Castillo AL, Toledano M. Polymer nanocarriers for dentin adhesion. J Dent Res 2014;93:1258–63. https://doi.org/10.1177/ 0022034514551608.
- [17] Besinis A, van Noort R, Martin N. The use of acetone to enhance the infiltration of HA nanoparticles into a demineralized dentin collagen matrix. Dent Mater 2016; 32:385–93. https://doi.org/10.1016/j.dental.2015.11.010.
- [18] Grossi JRA, Deliberador TM, Giovanini AF, Zielak JC, Sebastiani A, Gonzaga CC, et al. Effects of local single dose administration of parathormone on the early stages of osseointegration: A pre-clinical study. J Biomed Mater Res B Appl Biomater 2022;110:1806–13. https://doi.org/10.1002/jbm.b.35038.

- [19] Guimarães GN, Rodrigues TL, de Souza AP, Line SR, Marques MR. Parathyroid hormone (1-34) modulates odontoblast proliferation and apoptosis via PKA and PKC-dependent pathways. Calcif Tissue Int 2014;95:275–81. https://doi.org/ 10.1007/s00223-014-9892-1.
- [20] Sun W, Sun W, Liu J, Zhou X, Xiao Y, Karaplis A, et al. Alterations in phosphorus, calcium and PTHrP contribute to defects in dental and dental alveolar bone formation in calcium-sensing receptor-deficient mice. Dev Camb Engl 2010;137: 985–92. https://doi.org/10.1242/dev.045898.
- [21] Guimarães GN, Cardoso GBC, Naves LZ, Correr-Sobrinho L, Line SRP, Marques MR. Short-term PTH administration increases dentine apposition and microhardness in mice. Arch Oral Biol 2012;57:1313–9. https://doi.org/10.1016/j. archoralbio.2012.03.007
- [22] Kim M-R, Choi S-H, Lee B-N, Min K-S, Hwang Y-C. Effect of parathyroid hormonerelated protein on odontogenic differentiation in human dental pulp cells. BMC Oral Health 2020;20:101. https://doi.org/10.1186/s12903-020-01085-8.
- [23] Swarthout JT, D'Alonzo RC, Selvamurugan N, Partridge NC. Parathyroid hormone-dependent signaling pathways regulating genes in bone cells. Gene 2002;282:1–17. https://doi.org/10.1016/s0378-1119(01)00798-3.
- [24] Yoshida W, Matsugami D, Murakami T, Bizenjima T, Imamura K, Seshima F, et al. Combined effects of systemic parathyroid hormone (1-34) and locally delivered neutral self-assembling peptide hydrogel in the treatment of periodontal defects: an experimental in vivo investigation. J Clin Periodo 2019;46:1030–40. https://doi. org/10.1111/jcpe.13170.
- [25] Wojda SJ, Donahue SW. Parathyroid hormone for bone regeneration. J Orthop Res 2018;36:2586–94. https://doi.org/10.1002/jor.24075.
- [26] Zhao L, Ito S, Arai A, Udagawa N, Horibe K, Hara M, et al. Odontoblast death drives cell-rich zone-derived dental tissue regeneration. Bone 2021;150:116010. https://doi.org/10.1016/j.bone.2021.116010.
- [27] Lavicky J, Kolouskova M, Prochazka D, Rakultsev V, Gonzalez-Lopez M, Steklikova K, et al. The development of dentin microstructure is controlled by the type of adjacent epithelium. J Bone Min Res 2022;37:323–39. https://doi.org/ 10.1002/jbmr.4471.
- [28] Chardin H, Acevedo AC, Septier D, Staub JF, Goldberg M. Effects of thyroparathyroidectomy and parathyroidectomy upon dentinogenesis: Part I: Light microscopy. Connect Tissue Res 1995;32:261–7. https://doi.org/10.3109/ 03008209509013732.
- [29] Nagaraj E, Kaur RP, Raghuram PH, Kumar PS. Multiple internal resorption in permanent teeth associated with hyperparathyroidism. Indian J Dent Res 2013;24: 128–31. https://doi.org/10.4103/0970-9290.114917.
- [30] Turnbull RS, Heersche JN, Tam CS, Howley TP. Parathyroid hormone stimulates dentin and bone apposition in the thyroparathyroidectomized rat in a dosedependent fashion. Calcif Tissue Int 1983;35:586–90. https://doi.org/10.1007/ BE02405088
- [31] Emam H, Leach D, Sun Z, Tee BC, Karatas B, Kim D-G, et al. The effect of parathyroid hormone analogues when added to mineralized bone xenografts. J Oral Implant 2020;46:372–9. https://doi.org/10.1563/aaid-joi-D-19-00016.
- [32] Lindsay R, Krege JH, Marin F, Jin L, Stepan JJ. Teriparatide for osteoporosis: importance of the full course. Osteoporos Int J Establ Result Coop Eur Found Osteoporos Natl Osteoporos Found USA 2016;27:2395–410. https://doi.org/ 10.1007/s00198-016-3534-6.
- [33] Yang L, Huang J, Yang S, Cui W, Wang J, Zhang Y, et al. Bone regeneration induced by local delivery of a modified PTH-derived peptide from nanohydroxyapatite/ chitosan coated true bone ceramics. ACS Biomater Sci Eng 2018;4:3246–58. https://doi.org/10.1021/acsbiomaterials.7b00780.
- [34] Tang J, Yan D, Chen L, Shen Z, Wang B, Weng S, et al. Enhancement of local bone formation on titanium implants in osteoporotic rats by biomimetic multilayered structures containing parathyroid hormone (PTH)-related protein. Biomed Mater Bristol Engl 2020:15:045011. https://doi.org/10.1088/1748-605X/ab7b3d.
- [35] Jung RE, Cochran DL, Domken O, Seibl R, Jones AA, Buser D, et al. The effect of matrix bound parathyroid hormone on bone regeneration. Clin Oral Implants Res 2007;18:319–25. https://doi.org/10.1111/j.1600-0501.2007.01342.x.
   [36] Arrighi I, Mark S, Alvisi M, von Rechenberg B, Hubbell JA, Schense JC. Bone
- [36] Arrighi I, Mark S, Alvisi M, von Rechenberg B, Hubbell JA, Schense JC. Bone healing induced by local delivery of an engineered parathyroid hormone prodrug. Biomaterials 2009;30:1763–71. https://doi.org/10.1016/j. biomaterials 2008 12 023
- [37] Özer T, Başlarlı Ö, Aktaş A, Barış E, Çelik HH, Ocak M. Locally administrated single-dose teriparatide affects critical-size rabbit calvarial defects: a histological, histomorphometric and micro-CT study. Acta Orthop Trauma Turc 2019;53: 478–84. https://doi.org/10.1016/j.aott.2019.08.007.
- [38] Kajii F, Iwai A, Tanaka H, Matsui K, Kawai T, Kamakura S. Single-dose local administration of teriparatide with a octacalcium phosphate collagen composite enhances bone regeneration in a rodent critical-sized calvarial defect. J Biomed Mater Res B Appl Biomater 2018;106:1851–7. https://doi.org/10.1002/jbm. b.33993.
- [39] Wojda SJ, Marozas IA, Anseth KS, Yaszemski MJ, Donahue SW. Impact of release kinetics on efficacy of locally delivered parathyroid hormone for bone regeneration applications. Tissue Eng Part A 2021;27:246–55. https://doi.org/10.1089/ten. TEA 2020.0119.
- [40] Zaugg LK, Banu A, Walther AR, Chandrasekaran D, Babb RC, Salzlechner C, et al. Translation approach for dentine regeneration using GSK-3 antagonists. J Dent Res 2020;99:544–51. https://doi.org/10.1177/0022034520908593.
- [41] Medina-Castillo AL. Thermodynamic principles of precipitation polymerization and role of fractal nanostructures in the particle size control. Macromolecules 2020;53:5687–700. https://doi.org/10.1021/acs.macromol.0c00973.
- [42] Schaffazick SR, Pohlmann AR, Mezzalira G, Guterres SS. Development of nanocapsule suspensions and nanocapsule spray-dried powders containing

- melatonin. J Braz Chem Soc 2006;17:562–9. https://doi.org/10.1590/S0103-50532006000300020
- [43] Zhang Z, Yu J, Yao C, Yang H, Huang C. New perspective to improve dentinadhesive interface stability by using dimethyl sulfoxide wet-bonding and epigallocatechin-3-gallate. Dent Mater 2020;36:1452–63. https://doi.org/ 10.1016/j.dental.2020.08.009.
- [44] Sadek FT, Braga RR, Muench A, Liu Y, Pashley DH, Tay FR. Ethanol wet-bonding challenges current anti-degradation strategy. J Dent Res 2010;89:1499–504. https://doi.org/10.1177/0022034510385240.
- [45] Xu C, Wang Y. Collagen cross-linking increases its biodegradation resistance in wet dentin bonding. J Adhes Dent 2012;14:11–8. https://doi.org/10.3290/j.jad. 271404
- [46] Profeta AC, Mannocci F, Foxton R, Watson TF, Feitosa VP, De Carlo B, et al. Experimental etch-and-rinse adhesives doped with bioactive calcium silicate-based micro-fillers to generate therapeutic resin-dentin interfaces. Dent Mater 2013;29: 729–41. https://doi.org/10.1016/j.dental.2013.04.001.
- [47] Rahn BA, Perren SM. Xylenol orange, a fluorochrome useful in polychrome sequential labeling of calcifying tissues. Stain Technol 1971;46:125–9. https://doi. org/10.3109/10520297109067836.
- [48] Tzoumani I, Iatridi Z, Fidelli AM, Krassa P, Kallitsis JK, Bokias G. Room-Temperature Self-Healable Blends of Waterborne Polyurethanes with 2-Hydroxyethyl Methacrylate-Based Polymers. Int J Mol Sci 2023;24:2575. https://doi.org/ 10.3390/ijms24032575.
- [49] Sadeghi M, Heidari B. Crosslinked graft copolymer of methacrylic acid and gelatin as a novel hydrogel with pH-responsiveness properties. Materials 2011;4:543–52. https://doi.org/10.3390/ma4030543.
- [50] Tajiri T, Morita S, Ozaki Y. Hydration mechanism on a poly(methacrylic acid) film studied by in situ attenuated total reflection infrared spectroscopy. Polymer 2009; 50:5765–70. https://doi.org/10.1016/j.polymer.2009.09.060.
- [51] Lin H, Kai T, Freeman BD, Kalakkunnath S, Kalika DS. The effect of cross-linking on gas permeability in cross-linked poly(ethylene glycol diacrylate). Macromolecules 2005;38:8381–93. https://doi.org/10.1021/ma0510136.
- [52] Yu X, Wei M. Preparation and evaluation of parathyroid hormone incorporated CaP coating via a biomimetic method. J Biomed Mater Res B Appl Biomater 2011;97B: 345–54. https://doi.org/10.1002/jbm.b.31820.
- [53] McFarlane DR, McFarlane EF, Barden JA, Kemp BE. FTIR spectroscopy study of PTHrP(1–34) involved in humoral hypercalcaemia of malignancy. Biochim Biophys Acta BBA Protein Struct Mol Enzym 1993;1162:187–94. https://doi.org/ 10.1016/0167-4838(93)90146-I.
- [54] Van Meerbeek B, Vargas M, Inoue S, Yoshida Y, Perdigão J, Lambrechts P, et al. Microscopy investigations. Techniques, results, limitations. Am J Dent 2000;13: 3D–18D.
- [55] Sauro S, Pashley DH, Mannocci F, Tay FR, Pilecki P, Sherriff M, et al. Micropermeability of current self-etching and etch-and-rinse adhesives bonded to deep dentine: a comparison study using a double-staining/confocal microscopy technique. Eur J Oral Sci 2008;116:184–93. https://doi.org/10.1111/j.1600-0723-2007-05518 x
- [56] Toledano M, Cabello I, Aguilera FS, Osorio E, Toledano-Osorio M, Osorio R. Improved sealing and remineralization at the resin-dentin interface after phosphoric acid etching and load cycling. Microsc Micro 2015;21:1530–48. https://doi.org/10.1017/S1431927615015317.
- [57] D'Alpino P, Pereira J, Svizero N, Rueggeberg F, Pashley D. Factors affecting use of fluorescent agents in identification of resin-based polymers. J Adhes Dent 2006;8: 285
- [58] Toledano-Osorio M, Osorio E, Aguilera FS, Medina-Castillo AL, Toledano M,
   Osorio R. Improved reactive nanoparticles to treat dentin hypersensitivity. Acta Biomater 2018;72:371–80. https://doi.org/10.1016/j.actbio.2018.03.033.
   [59] Osorio R, Alfonso-Rodríguez CA, Medina-Castillo AL, Alaminos M, Toledano M.
- [59] Osorio R, Alfonso-Rodríguez CA, Medina-Castillo AL, Alaminos M, Toledano M. Bioactive polymeric nanoparticles for periodontal therapy. PloS One 2016;11: e0166217. https://doi.org/10.1371/journal.pone.0166217.
- [60] Vert M, Doi Y, Hellwich K-H, Hess M, Hodge P, Kubisa P, et al. Terminology for biorelated polymers and applications (IUPAC Recommendations 2012). Pure Appl Chem 2012;84:377–410. https://doi.org/10.1351/PAC-REC-10-12-04.
- [61] Boverhof DR, Bramante CM, Butala JH, Clancy SF, Lafranconi M, West J, et al. Comparative assessment of nanomaterial definitions and safety evaluation considerations. Regul Toxicol Pharm 2015;73:137–50. https://doi.org/10.1016/j. vrtpb.2015.06.001.
- [62] Gungormus M, Tulumbaci F. Peptide-assisted pre-bonding remineralization of dentin to improve bonding. J Mech Behav Biomed Mater 2021;113:104119. https://doi.org/10.1016/j.jmbbm.2020.104119.
- [63] Milly H, Festy F, Watson TF, Thompson I, Banerjee A. Enamel white spot lesions can remineralise using bio-active glass and polyacrylic acid-modified bio-active glass powders. J Dent 2014;42:158–66. https://doi.org/10.1016/j. ident 2013 11 012
- [64] Toledano M, Osorio E, Cabello I, Osorio R. Early dentine remineralisation: morphomechanical assessment. J Dent 2014;42:384–94. https://doi.org/10.1016/j. ident.2014.01.012.
- [65] Smith AJ, Scheven BA, Takahashi Y, Ferracane JL, Shelton RM, Cooper PR. Dentine as a bioactive extracellular matrix. Arch Oral Biol 2012;57:109–21. https://doi. org/10.1016/j.archoralbio.2011.07.008.
- [66] Xu Z, Neoh KG, Lin CC, Kishen A. Biomimetic deposition of calcium phosphate minerals on the surface of partially demineralized dentine modified with phosphorylated chitosan. J Biomed Mater Res B Appl Biomater 2011;98:150–9. https://doi.org/10.1002/jbm.b.31844.

- [67] Veis A, Dorvee JR. Biomineralization mechanisms: a new paradigm for crystal nucleation in organic matrices. Calcif Tissue Int 2013;93:307–15. https://doi.org/ 10.1007/s00223-012-9678-2.
- [68] Dey A, Bomans PHH, Müller FA, Will J, Frederik PM, de With G, et al. The role of prenucleation clusters in surface-induced calcium phosphate crystallization. Nat Mater 2010;9:1010-4. https://doi.org/10.1038/nmat2900.
- [69] Kim D-S, Kim J, Choi K-K, Kim S-Y. The influence of chlorhexidine on the remineralization of demineralized dentine. J Dent 2011;39:855–62. https://doi. org/10.1016/j.jdent.2011.09.010.
- [70] Clarkson BH, Feagin FF, McCurdy SP, Sheetz JH, Speirs R. Effects of phosphoprotein moieties on the remineralization of human root caries. Caries Res 1991;25:166–73. https://doi.org/10.1159/000261362.
- [71] Guimarães GN, Stipp RN, Rodrígues TL, de Souza AP, Line SRP, Marques MR. Evaluation of the effects of transient or continuous PTH administration to odontoblast-like cells. Arch Oral Biol 2013;58:638–45. https://doi.org/10.1016/j. archoralbio.2012.11.011
- [72] Pang X, Zhuang Y, Li Z, Jing S, Cai Q, Zhang F, et al. Intermittent Administration of Parathyroid Hormone Enhances Odonto/Osteogenic Differentiation of Stem Cells from the Apical Papilla via JNK and P38 MAPK Pathways. Stem Cells Int 2020; 2020:5128128. https://doi.org/10.1155/2020/5128128.
- [73] de Sousa JP, Carvalho RG, Barbosa-Martins LF, Torquato RJS, Mugnol KCU, Nascimento FD, et al. The Self-Assembling Peptide P11-4 Prevents Collagen Proteolysis in Dentin. J Dent Res 2019;98:347–54. https://doi.org/10.1177/ 0022034518817351.
- [74] Carvalho RG, Patekoski LF, Puppin-Rontani RM, Nakaie CR, Nascimento FD, Tersariol ILS. Self-assembled peptide P11-4 interacts with the type I collagen Cterminal telopeptide domain and calcium ions. Dent Mater 2023;39:708–17. https://doi.org/10.1016/j.dental.2023.06.004.
- [75] Rubin MR, Silverberg SJ, D'Amour P, Brossard J-H, Rousseau L, Sliney J, et al. An N-terminal molecular form of parathyroid hormone (PTH) distinct from hPTH(1 84) is overproduced in parathyroid carcinoma. Clin Chem 2007;53:1470–6. https://doi.org/10.1373/clinchem.2007.085506.
- [76] Han J-W, Lee B-N, Kim S-M, Koh J-T, Min K-S, Hwang Y-C. Odontogenic potential of parathyroid hormone-related protein (107-111) alone or in combination with mineral trioxide aggregate in human dental pulp cells. J Endod 2017;43:2054–60. https://doi.org/10.1016/j.joen.2017.08.016.
- [77] Marigo L, Migliaccio S, Monego G, La Torre G, Somma F, Ranelletti FO. Expression of parathyroid hormone-related protein in human inflamed dental pulp. Eur Rev Med Pharm Sci 2010;14:471–5.
- [78] Toledano M, Aguilera FS, Fernández-Romero E, Lagos AJ, Bonilla M, Lynch CD, et al. Dentin remineralization using a stimuli-responsive engineered small molecule GSK3 antagonists-functionalized adhesive. Dent Mater 2024;40:393–406. https://doi.org/10.1016/j.dental.2023.12.010.
- [79] Patil P, Banga KS, Pawar AM, Pimple S, Ganeshan R. Influence of root canal obturation using gutta-percha with three different sealers on root reinforcement of endodontically treated teeth. An in vitro comparative study of mandibular incisors. J Conserv Dent JCD 2017;20:241–4. https://doi.org/10.4103/JCD.JCD 233 16.
- [80] Posner AS, Blumenthal NC, Boskey AL. Model of aluminum-induced osteomalacia: inhibition of anatire formation and growth Kidney Int Suppl 1986;18:S17\_0
- inhibition of apatite formation and growth. Kidney Int Suppl 1986;18:S17–9.

  [81] Li X, Yu Z, Jiang S, Dai X, Wang G, Wang Y, et al. An amelogenin-based peptide hydrogel promoted the odontogenic differentiation of human dental pulp cells. Regen Biomater 2022;9:rbac039. https://doi.org/10.1093/rb/rbac039.

- [82] Oxlund H, Barckman M, Ørtoft G, Andreassen TT. Reduced concentrations of collagen cross-links are associated with reduced strength of bone. Bone 1995;17: S365–71. https://doi.org/10.1016/8756-3282(95)00328-B.
- [83] Li Y, Thula TT, Jee S, Perkins SL, Aparicio C, Douglas EP, et al. Biomimetic Mineralization of Woven Bone-Like Nanocomposites: Role of Collagen Cross-Links. Biomacromolecules 2012;13:49–59. https://doi.org/10.1021/bm201070g.
- [84] Sauro S, Osorio R, Osorio E, Watson TF, Toledano M. Novel light-curable materials containing experimental bioactive micro-fillers remineralise mineral-depleted bonded-dentine interfaces. J Biomater Sci Polym Ed 2013;24:940–56. https://doi. org/10.1080/09205063.2012.727377.
- [85] Sauro S, Osorio R, Watson TF, Toledano M. Therapeutic effects of novel resin bonding systems containing bioactive glasses on mineral-depleted areas within the bonded-dentine interface. J Mater Sci Mater Med 2012;23:1521–32. https://doi. org/10.1007/s10856-012-4606-6.
- [86] Pawley J. Fundamental Limits in Confocal Microscopy. In: Pawley JB, editor. Handb. Biol. Confocal Microsc. Boston, MA: Springer US; 1990. p. 15–26. https://doi.org/10.1007/978-1-4615-7133-9 2.
- [87] Griffiths B, Watson T, Sherriff M. The influence of dentine bonding systems and their handling characteristics on the morphology and micropermeability of the dentine adhesive interface. J Dent 1999;27:63–71.
- [88] Terzi A, Storelli E, Bettini S, Sibillano T, Altamura D, Salvatore L, et al. Effects of processing on structural, mechanical and biological properties of collagen-based substrates for regenerative medicine. Sci Rep 2018;8:1429. https://doi.org/ 10.1038/s41598-018-19786-0.
- [89] Tay FR, Pashley DH. Have dentin adhesives become too hydrophilic? J Can Dent Assoc 2003:69:726–31.
- [90] Padovano JD, Ravindran S, Snee PT, Ramachandran A, Bedran-Russo AK, George A. DMP1-derived peptides promote remineralization of human dentin. J Dent Res 2015;94:608–14. https://doi.org/10.1177/0022034515572441.
- [91] Bertassoni LE, Stankoska K, Swain MV. Insights into the structure and composition of the peritubular dentin organic matrix and the lamina limitans. Micron Oxf Engl 1993 2012;43:229–36. https://doi.org/10.1016/j.micron.2011.08.003.
- [92] Zurick KM, Qin C, Bernards MT. Mineralization induction effects of osteopontin, bone sialoprotein, and dentin phosphoprotein on a biomimetic collagen substrate. J Biomed Mater Res A 2013;101A:1571–81. https://doi.org/10.1002/jbm. a.34462.
- [93] Niu L-N, Zhang W, Pashley DH, Breschi L, Mao J, Chen J-H, et al. Biomimetic remineralization of dentin. Dent Mater 2014;30:77–96. https://doi.org/10.1016/j. dental.2013.07.013.
- [94] Sauro S, Osorio R, Watson TF, Toledano M. Influence of phosphoproteins' biomimetic analogs on remineralization of mineral-depleted resin-dentin interfaces created with ion-releasing resin-based systems. Dent Mater 2015;31:759–77. https://doi.org/10.1016/j.dental.2015.03.013.
- [95] Spencer P, Ye Q, Park J, Topp EM, Misra A, Marangos O, et al. Adhesive/Dentin interface: the weak link in the composite restoration. Ann Biomed Eng 2010;38: 1989–2003. https://doi.org/10.1007/s10439-010-9969-6.
- [96] Toledano M, Osorio R, Osorio E, Medina-Castillo AL, Toledano-Osorio M, Aguilera FS. Ions-modified nanoparticles affect functional remineralization and energy dissipation through the resin-dentin interface. J Mech Behav Biomed Mater 2017;68:62–79. https://doi.org/10.1016/j.jmbbm.2017.01.026.